EUROPEAN LABORATORY FOR PARTICLE PHYSICS (CERN)

CERN-EP/99-105
July 29, 1999

Inclusive Production of π^0, η, $\eta'(958)$, K^0_S and Λ in Two- and Three-Jet Events from Hadronic Z Decays

The ALEPH Collaboration[1]

Abstract

The production rates and the inclusive cross sections of the isovector meson π^0, the isoscalar mesons η and $\eta'(958)$, the strange meson K^0_S and the Λ baryon have been measured as functions of scaled energy in hadronic events, two-jet events and each jet of three-jet events from hadronic Z decays and compared to Monte Carlo models. The analysis is based on 3.7 million hadronic events collected with the ALEPH detector at LEP at a centre-of-mass energy of $\sqrt{s} = 91.2$ GeV. The JETSET modelling of the gluon fragmentation into isoscalar mesons is found to be in agreement with the experimental results. HERWIG fails to describe the K^0_S spectra in gluon-enriched jets and the Λ spectra in quark jets.

To be submitted to European Physical Journal C

[1]See next pages for the list of authors

The ALEPH Collaboration

R. Barate, D. Decamp, P. Ghez, C. Goy, J.-P. Lees, E. Merle, M.-N. Minard, B. Pietrzyk

Laboratoire de Physique des Particules (LAPP), IN^{2}P^3-CNRS, F-74019 Annecy-le-Vieux Cedex, France

R. Alemany, M.P. Casado, M. Chmeissani, J.M. Crespo, E. Fernandez, M. Fernandez-Bosman, Ll. Garrido,[15] E. Graugès, A. Juste, M. Martinez, G. Merino, R. Miquel, Ll.M. Mir, A. Pacheco, I.C. Park, I. Riu

Institut de Física d'Altes Energies, Universitat Autònoma de Barcelona, E-08193 Bellaterra (Barcelona), Spain[7]

A. Colaleo, D. Creanza, M. de Palma, G. Iaselli, G. Maggi, M. Maggi, S. Nuzzo, A. Ranieri, G. Raso, F. Ruggieri, G. Selvaggi, L. Silvestris, P. Tempesta, A. Tricomi,[3] G. Zito

Dipartimento di Fisica, INFN Sezione di Bari, I-70126 Bari, Italy

X. Huang, J. Lin, Q. Ouyang, T. Wang, Y. Xie, R. Xu, S. Xue, J. Zhang, L. Zhang, W. Zhao

Institute of High-Energy Physics, Academia Sinica, Beijing, The People's Republic of China[8]

D. Abbaneo, U. Becker,[19] G. Boix,[6] M. Cattaneo, F. Cerutti, V. Ciulli, G. Dissertori, H. Drevermann, R.W. Forty, M. Frank, T.C. Greening, A.W. Halley, J.B. Hansen, J. Harvey, P. Janot, B. Jost, I. Lehraus, O. Leroy, P. Mato, A. Minten, A. Moutoussi, F. Ranjard, L. Rolandi, D. Schlatter, M. Schmitt,[20] O. Schneider,[2] P. Spagnolo, W. Tejessy, F. Teubert, I.R. Tomalin, E. Tournefier, A.E. Wright

European Laboratory for Particle Physics (CERN), CH-1211 Geneva 23, Switzerland

Z. Ajaltouni, F. Badaud, G. Chazelle, O. Deschamps, A. Falvard, C. Ferdi, P. Gay, C. Guicheney, P. Henrard, J. Jousset, B. Michel, S. Monteil, J-C. Montret, D. Pallin, P. Perret, F. Podlyski

Laboratoire de Physique Corpusculaire, Université Blaise Pascal, IN^{2}P^3-CNRS, Clermont-Ferrand, F-63177 Aubière, France

J.D. Hansen, J.R. Hansen, P.H. Hansen, B.S. Nilsson, B. Rensch, A. Wäänänen

Niels Bohr Institute, DK-2100 Copenhagen, Denmark[9]

G. Daskalakis, A. Kyriakis, C. Markou, E. Simopoulou, I. Siotis, A. Vayaki

Nuclear Research Center Demokritos (NRCD), GR-15310 Attiki, Greece

A. Blondel, G. Bonneaud, J.-C. Brient, A. Rougé, M. Rumpf, M. Swynghedauw, M. Verderi, H. Videau

Laboratoire de Physique Nucléaire et des Hautes Energies, Ecole Polytechnique, IN^{2}P^3-CNRS, F-91128 Palaiseau Cedex, France

E. Focardi, G. Parrini, K. Zachariadou

Dipartimento di Fisica, Università di Firenze, INFN Sezione di Firenze, I-50125 Firenze, Italy

R. Cavanaugh, M. Corden, C. Georgiopoulos

Supercomputer Computations Research Institute, Florida State University, Tallahassee, FL 32306-4052, USA [13,14]

A. Antonelli, G. Bencivenni, G. Bologna,[4] F. Bossi, P. Campana, G. Capon, V. Chiarella, P. Laurelli, G. Mannocchi,[1,5] F. Murtas, G.P. Murtas, L. Passalacqua, M. Pepe-Altarelli[1]

Laboratori Nazionali dell'INFN (LNF-INFN), I-00044 Frascati, Italy

L. Curtis, J.G. Lynch, P. Negus, V. O'Shea, C. Raine, P. Teixeira-Dias, A.S. Thompson

Department of Physics and Astronomy, University of Glasgow, Glasgow G12 8QQ,United Kingdom[10]

O. Buchmüller, S. Dhamotharan, C. Geweniger, P. Hanke, G. Hansper, V. Hepp, E.E. Kluge, A. Putzer, J. Sommer, K. Tittel, S. Werner,[19] M. Wunsch

Institut für Hochenergiephysik, Universität Heidelberg, D-69120 Heidelberg, Germany[16]

R. Beuselinck, D.M. Binnie, W. Cameron, P.J. Dornan,[1] M. Girone, S. Goodsir, E.B. Martin, N. Marinelli, A. Sciabà, J.K. Sedgbeer, E. Thomson, M.D. Williams

Department of Physics, Imperial College, London SW7 2BZ, United Kingdom[10]

V.M. Ghete, P. Girtler, E. Kneringer, D. Kuhn, G. Rudolph

Institut für Experimentalphysik, Universität Innsbruck, A-6020 Innsbruck, Austria[18]

C.K. Bowdery, P.G. Buck, A.J. Finch, F. Foster, G. Hughes, R.W.L. Jones, N.A. Robertson, M.I. Williams

Department of Physics, University of Lancaster, Lancaster LA1 4YB, United Kingdom[10]

I. Giehl, K. Jakobs, K. Kleinknecht, G. Quast, B. Renk, E. Rohne, H.-G. Sander, H. Wachsmuth, C. Zeitnitz

Institut für Physik, Universität Mainz, D-55099 Mainz, Germany[16]

J.J. Aubert, C. Benchouk, A. Bonissent, J. Carr,[1] P. Coyle, F. Etienne, F. Motsch, P. Payre, D. Rousseau, M. Talby, M. Thulasidas

Centre de Physique des Particules, Faculté des Sciences de Luminy, IN^{2}P^3-CNRS, F-13288 Marseille, France

M. Aleppo, M. Antonelli, F. Ragusa

Dipartimento di Fisica, Università di Milano e INFN Sezione di Milano, I-20133 Milano, Italy

V. Büscher, H. Dietl, G. Ganis, K. Hüttmann, G. Lütjens, C. Mannert, W. Männer, H.-G. Moser, S. Schael, R. Settles, H. Seywerd, H. Stenzel, W. Wiedenmann, G. Wolf

Max-Planck-Institut für Physik, Werner-Heisenberg-Institut, D-80805 München, Germany[16]

P. Azzurri, J. Boucrot, O. Callot, S. Chen, A. Cordier, M. Davier, L. Duflot, J.-F. Grivaz, Ph. Heusse, A. Jacholkowska,[1] F. Le Diberder, J. Lefrançois, A.-M. Lutz, M.-H. Schune, J.-J. Veillet, I. Videau,[1] D. Zerwas

Laboratoire de l'Accélérateur Linéaire, Université de Paris-Sud, IN^{2}P^3-CNRS, F-91898 Orsay Cedex, France

G. Bagliesi, T. Boccali, C. Bozzi,[12] G. Calderini, R. Dell'Orso, I. Ferrante, L. Foà, A. Giassi, A. Gregorio, F. Ligabue, P.S. Marrocchesi, A. Messineo, F. Palla, G. Rizzo, G. Sanguinetti, G. Sguazzoni, R. Tenchini, A. Venturi, P.G. Verdini

Dipartimento di Fisica dell'Università, INFN Sezione di Pisa, e Scuola Normale Superiore, I-56010 Pisa, Italy

G.A. Blair, G. Cowan, M.G. Green, T. Medcalf, J.A. Strong

Department of Physics, Royal Holloway & Bedford New College, University of London, Surrey TW20 OEX, United Kingdom[10]

D.R. Botterill, R.W. Clifft, T.R. Edgecock, P.R. Norton, J.C. Thompson

Particle Physics Dept., Rutherford Appleton Laboratory, Chilton, Didcot, Oxon OX11 OQX, United Kingdom[10]

B. Bloch-Devaux, P. Colas, S. Emery, W. Kozanecki, E. Lançon, M.-C. Lemaire, E. Locci, P. Perez, J. Rander, J.-F. Renardy, A. Roussarie, J.-P. Schuller, J. Schwindling, A. Trabelsi,[21] B. Vallage

CEA, DAPNIA/Service de Physique des Particules, CE-Saclay, F-91191 Gif-sur-Yvette Cedex, France[17]

S.N. Black, J.H. Dann, R.P. Johnson, H.Y. Kim, N. Konstantinidis, A.M. Litke, M.A. McNeil, G. Taylor

Institute for Particle Physics, University of California at Santa Cruz, Santa Cruz, CA 95064, USA[22]

C.N. Booth, S. Cartwright, F. Combley, M. Lehto, L.F. Thompson

Department of Physics, University of Sheffield, Sheffield S3 7RH, United Kingdom[10]

K. Affholderbach, A. Böhrer, S. Brandt, C. Grupen, J. Hess, C. Koob, A. Misiejuk, G. Prange, U. Sieler
Fachbereich Physik, Universität Siegen, D-57068 Siegen, Germany[16]

G. Giannini, B. Gobbo
Dipartimento di Fisica, Università di Trieste e INFN Sezione di Trieste, I-34127 Trieste, Italy

J. Rothberg, S. Wasserbaech
Experimental Elementary Particle Physics, University of Washington, WA 98195 Seattle, U.S.A.

S.R. Armstrong, P. Elmer, D.P.S. Ferguson, Y. Gao, S. González, O.J. Hayes, H. Hu, S. Jin, J. Kile, P.A. McNamara III, J. Nielsen, W. Orejudos, Y.B. Pan, Y. Saadi, I.J. Scott, J. Walsh, J.H. von Wimmersperg-Toeller, Sau Lan Wu, X. Wu, G. Zobernig
Department of Physics, University of Wisconsin, Madison, WI 53706, USA[11]

[1]Also at CERN, 1211 Geneva 23, Switzerland.
[2]Now at Université de Lausanne, 1015 Lausanne, Switzerland.
[3]Also at Centro Siciliano di Fisica Nucleare e Struttura della Materia, INFN, Sezione di Catania, 95129 Catania, Italy.
[4]Also Istituto di Fisica Generale, Università di Torino, 10125 Torino, Italy.
[5]Also Istituto di Cosmo-Geofisica del C.N.R., Torino, Italy.
[6]Supported by the Commission of the European Communities, contract ERBFMBICT982894.
[7]Supported by CICYT, Spain.
[8]Supported by the National Science Foundation of China.
[9]Supported by the Danish Natural Science Research Council.
[10]Supported by the UK Particle Physics and Astronomy Research Council.
[11]Supported by the US Department of Energy, grant DE-FG0295-ER40896.
[12]Now at INFN Sezione de Ferrara, 44100 Ferrara, Italy.
[13]Supported by the US Department of Energy, contract DE-FG05-92ER40742.
[14]Supported by the US Department of Energy, contract DE-FC05-85ER250000.
[15]Permanent address: Universitat de Barcelona, 08208 Barcelona, Spain.
[16]Supported by the Bundesministerium für Bildung, Wissenschaft, Forschung und Technologie, Germany.
[17]Supported by the Direction des Sciences de la Matière, C.E.A.
[18]Supported by Fonds zur Förderung der wissenschaftlichen Forschung, Austria.
[19]Now at SAP AG, 69185 Walldorf, Germany.
[20]Now at Harvard University, Cambridge, MA 02138, U.S.A.
[21]Now at Département de Physique, Faculté des Sciences de Tunis, 1060 Le Belvédère, Tunisia.
[22]Supported by the US Department of Energy, grant DE-FG03-92ER40689.

1 Introduction

The description of the hadronization process in QCD is deeply connected with the confinement property and requires nonperturbative methods which are not available. The precise measurement of identified hadron spectra in the clean environment of e^+e^- annihilation into hadrons may improve the understanding of hadronization. Meanwhile, these measurements are necessary to test and tune the phenomenological models used to describe hadronization; each of these models has free parameters which must be determined from comparison with data.

Some more insights into the hadronization process may be obtained from the analysis of the individual jets in hadronic events. The observed hadron jets can be associated with the quark and gluon jets and thus quark and gluon fragmentation can be studied. The higher effective color charge for gluon splitting together with the assumption that hadron multiplicity is proportional to parton multiplicity (so-called Local Parton-Hadron Duality [1]) lead to the prediction of a higher particle multiplicity and a softer fragmentation function in gluon jets than quark jets. Conclusive results which support these predictions have recently been obtained at LEP [2], mainly using charged particles. Further details may be revealed by studying identified hadrons produced in quark and gluon jets. They could explain the discrepancies between the measured values and models observed in the shape of the inclusive cross sections for certain strange mesons and baryons [2].

For isoscalar mesons (η, $\eta'(958)$, $\omega(782)$, $\phi(1020)$), there are some theoretical models which predict an enhancement in gluon jets compared to quark jets of the same energy in addition to that due to the higher color charge of the gluon. In some of the models, these predictions are based on particular gluon fragmentation schemes. For example, only isoscalar mesons are produced directly when a gluon fragments [3], or an explicit recombination function for a particular hadron is convolved with a parton probability function for partons from a parton shower at a given Q_0 cutoff [4–7]. In other models, they are based on the "leading particle" effect [8] combined with the assumption that the isoscalar mesons contain a significant gg component [9]. Gluon jets are also expected [10] to exhibit an anomalously large tendency to fragment into $\eta'(958)$ mesons due to the large coupling of $\eta'(958)$ mesons to gluonic field configurations expected from the QCD (strong) anomaly solution of the $U(1)$ problem. The additional enhancement of isoscalars in gluon jets should manifest itself particularly at higher momenta.

Experimental searches for the effects predicted by these models were performed in e^+e^- annihilations by ARGUS [11] and Crystal Ball [12] at $\sqrt{s} = 10$ GeV and by JADE [13] at $\sqrt{s} = 34$ GeV. No particular enrichment was observed for isoscalars in gluon jets, but the statistics were rather low and the quark and gluon jets were selected in different environments. At LEP, the L3 experiment [14] measured the η production rates in two- and three-jet events from hadronic Z decays and found that the measured momentum spectrum in the lowest-energy jet (gluon-enriched) in three-jet events is harder than that of the HERWIG and JETSET models, while the description of the first two energy-ordered jets (quark-enriched) is satisfactory. OPAL [15] have measured the production rate of $\phi(1020)$

mesons in each jet of three-jet events; jets were ordered according to their energies. The measured values are in good agreement with JETSET for all three jets.

In this analysis, the production rates and the inclusive cross sections of the isovector meson π^0, the isoscalar mesons η and $\eta'(958)$, the strange meson K^0_S and the Λ baryon are determined in hadronic events, two-jet events and each jet of three-jet events from hadronic Z decays. The measured quantities are compared with the values computed with the JETSET 7.4 [16], HERWIG 5.8 [17] and ARIADNE 4.08 [18] Monte Carlo (MC) models. Jets in two-jet events correspond to quark jets, in lowest order of perturbation theory. In three-jet events with jets ordered according to their energies, the first two jets are quark-enriched and the third is gluon-enriched. In this way, spectra measured separately in quark- and gluon-enriched jets can be compared with the corresponding spectra of the MC models.

For isoscalar particles, the additional enhancement in gluon jets predicted by the theoretical models described above is not implemented in JETSET or HERWIG; it should therefore appear in the spectra of η and $\eta'(958)$ in gluon-enriched jets as a deviation at high momenta from the MC values. No deviation should appear for the directly produced π^0 isovector meson in gluon-enriched jets.

2 The ALEPH detector

A detailed description of the ALEPH detector can be found in [19]; the performance of the detector is reviewed in [20].

The tracking system consists of three subdetectors: a vertex detector, composed of two layers of double-sided microstrip detectors, surrounded by an inner drift chamber giving typically eight $r\phi$ points and by a time projection chamber (TPC) which provides up to 21 three-dimensional space-points and up to 338 measurements of the specific ionization density $\mathrm{d}E/\mathrm{d}x$ of a track. The tracking is located inside a 1.5 T superconducting solenoid. The transverse momentum resolution of the whole tracking system is $\sigma(1/p_T) = 0.6 \times 10^{-3}\,(\mathrm{GeV}/c)^{-1}$; at low momentum, multiple scattering dominates and adds a constant term of 0.005 to $\sigma(p_T)/p_T$.

The electromagnetic calorimeter (ECAL) is also inside the coil and is formed of a barrel surrounding the time projection chamber and two endcaps. It has 45 lead/proportional-chamber layers segmented into 74000 projective towers, corresponding to an average granularity of $0.9^\circ \times 0.9^\circ$. Each tower is read out in three storeys in depth, corresponding respectively to 4, 9 and 9 radiation lengths. The energy resolution of ECAL is $\sigma(E)/E = 0.18/\sqrt{E/(\mathrm{GeV})}+0.009$ and the angular resolution is $\sigma_{\theta,\phi} = (2.5/\sqrt{E/(\mathrm{GeV})}+0.25)$ mrad.

The hadronic calorimeter (HCAL) consists of 23 layers of plastic streamer tubes, separated by 5 cm thick iron slabs. It is used together with ECAL to measure hadronic energy deposits. Completed with two double-layers of streamer tubes on the outside of ALEPH, it forms the muon identification system.

The charged tracks are reconstructed starting from the TPC, then extrapolating the candidate tracks to the inner detectors where consistent hits are assigned; the set of

preliminary track parameters obtained in this way is used in the final track fit, based on Kalman filter techniques, which also includes the multiple scattering between each measurement.

The photons are reconstructed using the energy deposited in the electromagnetic calorimeter. The storeys of the three segments in depth are grouped into clusters by means of an algorithm which takes into account the shape expected for an electromagnetic shower. The photon energy is computed from the energy collected in the four central towers of a cluster and the expected value of the fraction of energy in the four towers. Corrections are computed for energy losses before and after the calorimeter and in the barrel-endcap overlap region.

The energy flow of an event can be obtained as the sum of the energy found in all calorimeter cells; this method yields a resolution of $\sigma(E)/E = 1.2/\sqrt{E/(\mathrm{GeV})}$ for hadronic Z decays. This resolution is improved by making use of the particle identification capabilities of the detector and avoiding the double counting of energy. A consistent set of "energy-flow objects" [20] (electrons, muons, photons, and neutral and charged hadrons) characterized by their energies and momenta is obtained in this way and the resolution on the energy flow of an event is $\sigma(E) = (0.59 \pm 0.03)\sqrt{E/(\mathrm{GeV})} + (0.6 \pm 0.3)$ GeV.

3 Event selection

The analyses are based on 3.5 million hadronic events recorded by the ALEPH detector at the Z peak (centre-of-mass energy $\sqrt{s} = 91.2$ GeV) during the 1992-1995 running of LEP. For the K^0_S and Λ analyses, data from the 1991 running are also used, giving an additional 238 000 events.

The selection of hadronic events is done with the standard criteria used in ALEPH [21]. Each selected event should have at least five good charged tracks, with a total energy greater than 10% of the centre-of-mass energy. A good charged track has at least four measured points in the TPC, a distance of closest approach of the extrapolated track to the beam line smaller than 2 cm in $r\phi$ and 10 cm in z, and a polar angle θ with $|\cos\theta| < 0.95$.

Additional criteria are imposed to ensure well-contained events. The event is required to have at least 15 energy-flow objects, a visible energy in excess of 45.6 GeV, and the polar angle of the thrust axis computed using the energy-flow objects between 30° and 150° with respect to the beam axis.

The jets are clustered from all energy-flow objects using the $k_\perp$ (Durham) algorithm [22] with the E recombination scheme and a jet resolution parameter of $y_\mathrm{cut} = 0.01$. Of the events, 63.9% were clustered as two-jet events, 30.6% as three-jet events and the other 5.5% of the events have more than three jets. The polar angle between each jet and the beam axis is required to be between 30° and 150°. From the three-jet event sample, the events which have one or more jets with more than 85% of the visible jet energy carried by a single photon are rejected as possible $q\overline{q}\gamma$ events. The final samples consist of 1.8 million two-jet events and 719 000 three-jet events (about 2 million and 0.8 million, respectively, when data from 1991 are included). The events with more than three jets are not considered

in these analyses.

For three-jet events, the jet energies are recomputed from their directions, assuming planar, massless kinematics; the jet-energy resolution is improved using this procedure due to the better angular resolution compared to the energy resolution of the ALEPH detector. Jets are then ordered according to the recomputed energies. The average $x_{\rm jet} = E_{\rm jet}/E_{\rm beam}$ is 0.93 for jet 1, 0.72 for jet 2, and 0.35 for jet 3.

The MC events, used to correct for detector effects, are generated using the JETSET parton shower model, with modified charm and bottom decay tables and generation of initial state radiation (ISR) photons with DYMU3 [23]; these events are passed through the full ALEPH detector simulation, subjected to the same cuts and analyzed in the same way as the data.

Good agreement between the jet rates and the jet energies in data and MC events is obtained using the Durham algorithm with $y_{\rm cut} = 0.01$. The rates of two- and three-jet events in the MC sample are 62.3% and 32.5%. The average jet energies are the same as in data within 1%. The hadronization corrections to parton jet rates are also small for this value of the resolution parameter.

In MC events, the reconstructed jets are matched with the parton jets which are nearest in angle. It is found that, on average, jet 1 (jet 2) is a quark or antiquark jet in 96% (75%) of the cases and that the third jet originates from a gluon with 71% probability. The gluon probability is however a function of the jet energy, decreasing with jet energy (from ∼90% at 5 GeV to ∼50% at 25 GeV), while the quark content increases with jet energy.

4 Data analysis

4.1 Reconstruction of π^0 and η mesons

The π^0 and the η mesons are analyzed using the $\gamma\gamma$ decay channel with branching ratios of 98.8% for π^0 and 39.2% for η. In two- and three-jet events, both photons from a $\gamma\gamma$ combination are required to belong to the same jet.

The photons are reconstructed as neutral clusters in the electromagnetic calorimeter. The following supplementary criteria are imposed on the identified photons. To reduce the hadronic contamination, the fraction $R_1 + R_2$ of their energy in the first two segments in depth of the ECAL should be greater than 0.8, and the fraction F_4 of their energy in the four central towers of the shower should be greater than 0.8. The energy of the photon candidates should be greater than 1 GeV. In addition, for the η analysis the photon pairs with invariant mass within 40 MeV/c^2 of the π^0 mass are rejected and a cut on the photon energy $E_\gamma > 1.75$ GeV is imposed.

The invariant mass $M_{\gamma\gamma}$ of the $\gamma\gamma$ pairs is obtained in several intervals of $x = E_{\gamma\gamma}/E_{\rm beam}$. For each x interval, the number of η candidates is determined by fitting the invariant mass distribution with the sum of a Gaussian for the signal and a quartic polynomial for the background. For π^0 fits, the sum of a distorted Gaussian and a Fermi-like function is used. In the distorted Gaussian function, the skewness terms $-(1/2)s\delta + (1/6)s\delta^3$ are added to

the Gaussian exponent, with $\delta = M_{\gamma\gamma} - \mu$, s the skewness coefficient and μ the mean value. The Fermi-like function is $f_{\rm bg}(M_{\gamma\gamma}) = [b_3 + b_4(M_{\gamma\gamma} - b_1)]/\{1 + \exp[(b_1 - M_{\gamma\gamma})/b_2]\}$. Examples of π^0 and η mass distributions are shown in Figs. 1 and 2.

The reconstruction efficiency for π^0 has a strong dependence on the pion energy, with a maximum around 10 GeV. It varies between 0.2 and 0.5 as a function of x. For η the efficiency increases typically from 0.05 to 0.20 as a function of x. The branching ratios π^0 , $\eta \to \gamma\gamma$ are included in these values.

4.2 Reconstruction of $\eta'(958)$ mesons

The $\eta'(958)$ analysis is performed using the $\eta'(958) \to \eta\pi^+\pi^-$ decay channel, with a branching ratio of 43.8%.

Photon pairs with invariant mass within 100 MeV/c^2 of the fitted η mass are taken as η candidates; for these pairs, the mass is constrained to the nominal η mass.

The pions are selected from the energy-flow objects as charged tracks which have at least five coordinates in the TPC, originate from a cylindrical region of radius 1 cm and half-length 5 cm centred on the nominal interaction point, have a polar angle with respect to the beam axis in the range $20^\circ \leq \theta \leq 160^\circ$ and a transverse momentum greater than 0.2 GeV/c. The charged tracks identified as electrons or muons [20] are rejected from the pion candidate sample.

In two- and three-jet events, all three particle candidates from an $\eta\pi^+\pi^-$ combination are required to belong to the same jet.

The invariant mass distributions of the $\eta\pi^+\pi^-$ combinations are obtained as a function of the scaled energy $x = E_{\eta\pi^+\pi^-}/E_{\rm beam}$ and are fitted for each x bin with the sum of a Gaussian function for the signal and a cubic polynomial for the background. An example of an $\eta'(958)$ mass distribution is shown in Fig. 3.

The reconstruction efficiency for $\eta'(958)$ increases typically from 0.025 to 0.075 as a function of x. The branching ratios $\eta \to \gamma\gamma$ and $\eta'(958) \to \eta\pi^+\pi^-$ are included in these values.

4.3 Reconstruction of $\mathbf{K^0_S}$ and $\mathbf{\Lambda/\overline{\Lambda}}$

The $\rm K^0_S$ mesons are reconstructed from their decay into two charged pions with a branching ratio of 68.6%, while the Λ ($\overline{\Lambda}$) baryons are reconstructed from their decay into a proton and a charged pion with a branching ratio of 63.9%. The selection cuts applied for $\rm V^0$ candidates are similar to those in the previously published analysis of $\rm K^0_S$ and Λ production in hadronic events [24]: all pairs of oppositely charged tracks in an event are tested for the hypothesis that they originate from a common secondary vertex and their measured specific ionizations are required to be consistent with those expected for the decay particles. Pairs consistent with being photon conversions are rejected. The reconstructed $\rm V^0$'s are assigned to the jet with the smallest angle with respect to their direction of flight.

The invariant masses of the pairs of charged tracks are calculated in intervals of the scaled momentum $x_p = p_{\rm hadron}/p_{\rm beam}$. In each interval the invariant mass distribution is

fitted with the sum of a signal function and a background function. The signal is described for K^0_S mesons by the sum of two Gaussian functions, with the relative normalization and the relative width fixed from fully simulated MC events; a Breit-Wigner distribution is used for the Λ. In both cases, the background is described by a linear function. Examples of K^0_S and Λ mass distributions are shown in Figs. 4 and 5, respectively.

The reconstruction efficiency has a strong dependence on the V^0 momentum.Typically, it is 55% (50%) for $K^0 \to \pi^+\pi^-$ ($\Lambda \to p\pi^-$) at 8 GeV/c and drops below 30% for momenta smaller than 1.5 GeV/c or greater than 15 GeV/c.

4.4 Measurement of production rates

The inclusive normalized cross section f of each measured hadron h as a function of the x (x_p) variable is computed for each jet of the three-jet events using the relation

$$f^{\text{jet } i}(x) = \frac{1}{\sigma_3}\frac{\mathrm{d}\sigma}{\mathrm{d}x} = \frac{1}{N_{3\text{j}}^{\text{data}}}\,\frac{N_h^{\text{data, jet } i}(\text{rec})}{\Delta x}\,\frac{N_h^{\text{MC, jet } i}(\text{gen})}{N_h^{\text{MC, jet } i}(\text{rec})}\,, \tag{1}$$

where $N_h^{\text{data, jet } i}(\text{rec})$ is the number of reconstructed h particles in jet i in a given x bin for data (similarly for MC), Δx is the width of the x bin, and $N_h^{\text{MC, jet } i}(\text{gen})$ is the number of generated h particles in jet i in a given x bin for MC events without ISR, detector simulation or selection criteria, normalized to the same number of events as the MC sample with ISR, full detector simulation and selection cuts applied. For each jet, the cross section is normalized to the number of selected three-jet events $N_{3\text{j}}^{\text{data}}$. The analyzed particle is treated as stable in the jet clustering at the generator level. For K^0_S and Λ, the inclusive cross sections are also calculated as a function of $\xi = \ln(1/x_p)$; for π^0, η and $\eta'(958)$ mesons, the ξ distribution is not used because its maximum is not reached due to the relatively high cut on photon energy.

The cross section is also calculated for two-jet events normalized to the number of selected two-jet events $N_{2\text{j}}^{\text{data}}$, summing before fitting the invariant mass distributions in each x bin for the two jets, and for all hadronic events normalized to the number of hadronic events $N_{\text{had}}^{\text{data}}$.

5 Systematic errors

5.1 Systematic errors for π^0 and η mesons

The systematic errors on π^0 and η multiplicities and inclusive cross sections are obtained as the sum in quadrature of three components: from varying the cuts, varying the fit range and from the energy calibration of the ECAL.

The cuts on $R_1 + R_2$, F_4 and θ_{thrust} are replaced separately by: no cut on $R_1 + R_2$, no cut on F_4, and $45^\circ \leq \theta_{\text{thrust}} \leq 135^\circ$, respectively. For the η analysis, the cut on photon energy is also changed to $E_\gamma > 2$ GeV. For each x bin, the maximum difference between the nominal inclusive cross section and the values obtained with one cut changed is taken as

the systematic error. The relative error on the multiplicity coming from the cut variation is obtained conservatively as the linear sum over all the x bins of the relative errors on multiplicity in each bin, weighted by the multiplicity in that bin.

The fit range is varied, changing both the lower and upper limits by reasonable values. The error is taken to be the maximum difference between the nominal multiplicity in the measured x range and the ones obtained using different fit ranges. The systematic error on the inclusive cross section is computed assuming for each x bin the same relative error as that obtained above for the multiplicity measured in the whole accessible x range.

The calibration error for ECAL energy was assumed to be 2.5% for $E = 1$ GeV and 2.0% for $E = 1.75$ GeV. The systematic effects on the π^0 and η multiplicities given by these errors were computed from the relative difference in the number of selected photons.

5.2 Systematic errors for $\eta'(958)$ mesons

The systematic errors on the $\eta'(958)$ multiplicity are calculated from the selection criteria for η and $\pi^{\pm}$ candidates and from the variation of the fit range within reasonable limits. The error from the selection of η candidates is the sum in quadrature of the systematic errors from cut variation and ECAL calibration. The difference in the number of $\pi^{\pm}$ selected in data and MC is used to calculate the error from $\pi^{\pm}$ selection; the errors are added linearly for π^+ and π^- to allow for maximal correlations. The error from the fit range variation is obtained in the same way as for π^0 and η mesons. The three components are added in quadrature to give the total systematic error.

5.3 Systematic errors for K^0_S and Λ

The systematic errors for both K^0_S and Λ are dominated by the V^0 selection. They are studied by successively varying the cuts on: the specific ionization $\mathrm{d}E/\mathrm{d}x$, the quality of the vertex fit $\chi^2_{\text{vertex fit}}$, the decay length and the decay angle $\cos\theta^*$.

The variation of the event selection cuts has no significant influence on the results. Different schemes of V^0 assignment to the jets yield only very small effects. Using different signal and background functions give results consistent with statistical fluctuations.

6 Results

The inclusive cross sections of π^0, η, $\eta'(958)$ and K^0_S mesons and Λ baryons are determined in all hadronic events, two-jet events and each jet of three-jet events according to the procedure outlined in Section 4.4. They are compared with the values computed with JETSET 7.4, HERWIG 5.8 and ARIADNE 4.08 Monte Carlo models. For each particle analyzed, the multiplicity is obtained by integrating the inclusive cross section over the accessible x, x_p or ξ range.

The parameters of the MC models were tuned [25] to ALEPH event shape and single charged particle distributions and to ALEPH inclusive spectra of various particles

(including η, $\eta'(958)$, K^0_S and Λ) in hadronic events. The inclusive spectra in two- or three-jet events presented here were not used for tuning. In JETSET, an ad hoc $\eta'(958)$ suppression of 0.275 was imposed; no ad hoc suppression was required for η mesons. The suppression of the first rank di-quarks in b and c events has been turned off in JETSET to increase the fraction of $b \to \Lambda_b$ and $c \to \Lambda_c$ to agree with recent measurements by ALEPH [26]. In the model analysis of a particular particle type, the particles of that type are required to be stable. Jet energies are also recomputed from their directions, assuming planar, massless kinematics.

The multiplicities obtained are summarized in Table 1 for π^0, Table 3 for η, Table 5 for $\eta'(958)$, Table 7 for K^0 and Table 9 for Λ. For K^0_S mesons and Λ baryons, the measured values contribute more than 94% and 96%, respectively, to the total multiplicity, therefore only the values extrapolated to the full range using JETSET 7.4 are given in the tables. The multiplicity for K^0 ($K^0_S + K^0_L$) was taken as twice the K^0_S multiplicity. The systematic errors on multiplicities are summarized in Tables 2, 4, 6, 8 and 10 for π^0, η, $\eta'(958)$, K^0_S and Λ, respectively. For comparison, the corresponding statistical errors are also given in the same tables.

The measured π^0, η and $\eta'(958)$ inclusive cross sections as functions of the x variable are shown in Fig. 6a for all hadronic events, Fig. 6b for two-jet events, and Figs. 7, 8 and 9 for each jet in three-jet events. Figures 10 and 11 present the inclusive cross sections in all hadronic events for K^0_S and Λ, respectively, as functions of x_p and $\xi = \ln(1/x_p)$; for two-jet events, the inclusive cross sections are shown in Figs. 12 and 13. The inclusive cross sections in the first, the second and the third jet in three-jet events are shown in Figs. 14, 15 and 16 for K^0_S mesons, and in Figs. 17, 18 and 19 for Λ baryons. Also shown in the figures are the corresponding inclusive cross sections from the MC models. The numerical values of the π^0, η and $\eta'(958)$ inclusive cross sections are given in Tables 11, 12 and 13 for all hadronic events, Tables 14, 15 and 16 for two-jet events, and Tables 17, 18 and 19 for jets in three-jet events. For K^0_S and Λ, the numerical values are given in Tables 20 and 21 for hadronic events, and Tables 22 and 23 for two-jet events; for the first, the second and the third jet in three-jet events, the values are given in Tables 24, 25 and 26 for K^0_S, and Tables 27, 28 and 29 for Λ. ASCII files for the tables can be found at `http://alephwww.cern.ch/ALPUB/paper/paper_99.html` address.

7 Discussion

7.1 Discussion of π^0, η and $\eta'(958)$ results

For hadronic events and two-jet events (a subsample of $\approx 63\%$ of the hadronic events, after the additional cuts), the π^0, η and $\eta'(958)$ spectra computed with JETSET are found to be in reasonable agreement with the measured spectra, apart from the high $x > 0.75$ region where JETSET shows an excess of η particles. This latter region is very sensitive to the values of the fragmentation parameters and a similar discrepancy has been observed [25] for the charged particle distribution in hadronic events. In contrast, HERWIG shows a

slightly too steep dependence on x for η and $\eta'(958)$.

The π^0 inclusive cross sections for jets in the three-jet events are better reproduced by JETSET, with a slightly overestimated production at higher x for jet 1 and jet 2; HERWIG is in good agreement with the data for jet 1, but is not steep enough in x for jet 2 and too steep for jet 3. The agreement of both models with data can, however, be considered reasonable.

The measured η inclusive cross sections in jets of the three-jet events are well reproduced by JETSET for each jet. For a quantitative comparison between data and the phenomenological models, a

$$\chi^2 = \sum_{x\,\mathrm{bins}} \left[f_{\mathrm{model}}(x) - f_{\mathrm{data}}(x)\right]^2 / \left(\sigma_{\mathrm{tot}}^{\mathrm{data}}\right)^2$$

is defined for each jet and the ratio of χ^2 to the number of degrees of freedom (ndf) is computed. Here the total error $\sigma_{\mathrm{tot}}^{\mathrm{data}}$ is the sum in quadrature of the statistical and systematic errors on the measured value. For the third jet, which according to MC calculations represents the gluon jet in $\sim$71% of the cases, the χ^2/ndf is equal to 2.7/3. The other two jets are also reasonably well modelled, with χ^2/ndf equal to 5.3/5 for the second jet and 11.2/6 for the first jet. As in hadronic events and two-jet events, HERWIG shows a slightly too steep dependence on x for all three jets; the χ^2/ndf are 6.1/3 for the third jet, 12.8/5 for the second jet and 32.5/6 for the first jet.

For $\eta'(958)$ mesons, the measured inclusive cross sections and the measured multiplicities are reproduced by JETSET and HERWIG for each of the three jets, all the model values being within one σ_{tot} of the measured values.

Because reasonable agreement with the measured spectra in quark-enriched jets is observed for both isoscalar and isovector mesons and no significant deviations are observed for isoscalar mesons in gluon-enriched jets, one can conclude that the JETSET modelling of gluon fragmentation into isoscalar mesons is in agreement with the experimental results for the measured x region. No additional enhancement for isoscalar mesons in gluon jets, as predicted by the models mentioned in Section 1 and which would manifest as a deviation from the JETSET values, is observed in the experimental results.

The slightly too steep dependence on x shown by HERWIG for η spectra in two-jet events and each jet of three-jet events does not depend on the average gluon content of the jet. Therefore, these discrepancies cannot be related to particular effects of gluon fragmentation into isoscalar mesons.

Using the new spectra in hadronic events obtained here, the parameters describing η and $\eta'(958)$ production in the JETSET string model are examined again. The data are best described by the default value for the pseudoscalar mixing angle $\theta_P = -9.7^\circ$ and by an ad hoc $\eta'(958)$ suppression factor of 0.275. For a different value of the mixing angle, $\theta_P = -20^\circ$, the data still require a sizeable $\eta'(958)$ suppression of $\approx$0.40. No ad hoc η suppression is required.

7.2 Discussion of K^0_S and Λ results

The measured spectra are well reproduced by JETSET and ARIADNE in both quark(-enriched) jets (the first two jets in three-jet events and jets in two-jet events) and gluon-enriched jets; the agreement between the models and the data is also reasonable in all hadronic events.

HERWIG is in reasonable agreement with the measured spectra for K^0_S in jets with a high quark content (jets in two-jet events and the first jet in three-jet events), but gives fewer K^0_S mesons as the gluon content of the jet becomes significant; the discrepancy gets larger with the increase of the gluon content of the jet. As a consequence of the large discrepancies seen for the last two jets in three-jet events, HERWIG also gives fewer K^0_S mesons than measured in hadronic events.

In the Λ spectra, HERWIG has a shoulder which is not seen in the measured spectra. The shoulder decreases with the decrease of the quark content of the jet: it is very clear in two-jet events and in the first jet of three-jet events, smaller in the second jet of three-jet events and absent in the third jet of three-jet events. HERWIG gives also too many Λ's in jets with a high quark content and too few in the third jet of three-jet events, which has a high gluon content. The shoulder in jets with a high quark content is also shown by HERWIG in hadronic events and is not seen in the data; HERWIG also gives more Λ baryons than measured in hadronic events.

The new version HERWIG 5.9 does not improve the description of the data; the disagreements in the shapes of the momentum spectra are also observed with the new version.

8 Conclusions

The production rates and the inclusive cross sections of the isovector meson π^0, the isoscalar mesons η and $\eta'(958)$, the strange meson K^0_S and the Λ baryon were determined in hadronic events, two-jet events and each jet of three-jet events from Z decays. The measured quantities have been compared with the values computed with the tuned JETSET 7.4, HERWIG 5.8 and ARIADNE 4.08 models.

For all the particles analyzed, the inclusive cross sections are in agreement with previous ALEPH results [24, 25].

The measured spectra for the isovector meson π^0 are reasonably reproduced by JETSET and HERWIG. For the isoscalar mesons η and $\eta'(958)$, the measured spectra are well reproduced by JETSET for quark(-enriched) jets and gluon-enriched jets. Therefore, the JETSET description of gluon fragmentation into isoscalar mesons is in agreement with the experimental results for the measured x region. HERWIG shows a slightly too steep dependence on x for η spectra in two-jet events and each jet of three-jet events; these discrepancies cannot be related to gluon fragmentation into isoscalar mesons because they do not depend on the average gluon content of the jet.

The measured spectra for K^0_S and Λ hadrons are reproduced by JETSET and ARIADNE

in quark(-enriched) jets and in gluon-enriched jets. HERWIG fails to describe the K^0_S spectra in jets with a significant gluon content, giving too few K^0_S mesons; the discrepancies increase with the average gluon content. HERWIG also fails to describe the shape of the Λ spectra in jets with high quark content and overestimates the number of Λ's in these jets.

Acknowledgments

We wish to thank our colleagues from the accelerator divisions for the successful operation of the LEP machine, and the engineers and technical staff in all our institutes for their contribution to the good performance of ALEPH. Those of us from non-member states thank CERN for its hospitality.

References

[1] Ya.I. Azimov et al., Phys. Lett. B **165** (1985) 147, Z. Phys. C **27** (1985) 65.

[2] For a review see A. Böhrer, Phys. Rep. **291** (1997) 107, or
I.G. Knowles and G.D. Lafferty, J. Phys. G **23** (1997) 731.

[3] C. Peterson and T.F. Walsh, Phys. Lett. B **91** (1980) 455.

[4] K.P. Das and R.C. Hwa, Phys. Lett. B **68** (1977) 459.

[5] V. Chang and R.C. Hwa, Phys. Rev. D **23** (1981) 728.

[6] V. Chang, G. Eilam and R.C. Hwa, Phys. Rev. D **24** (1981) 1818.

[7] R. Migneron, L.M. Jones and K.E. Lassica, Phys. Rev. D **26** (1982) 2235.

[8] A. De Angelis, G. Cosmo and F. Cossutti, Int. J. Mod. Phys. C **6** (1995) 585.

[9] P. Ball, J.-M. Frère and M.Tytgat, Phys. Lett. B **365** (1996) 367.

[10] H. Fritzsch, Phys. Lett. B **415** (1997) 83.

[11] ARGUS Collaboration, *Physics with ARGUS*, Phys. Rep. **276** (1996) 223.

[12] Crystal Ball Collaboration, *Measurement of* π^0 *and* η *meson production in* e^+e^- *annihilation at* $\sqrt{s}$ *near 10* GeV, Z. Phys. C **49** (1991) 225.

[13] JADE Collaboration, *A study of photon production in hadronic* e^+e^- *annihilation*, Z. Phys. C **28** (1985) 343.

[14] L3 Collaboration, *Measurement of* η *production in two and three-jet events from hadronic* Z *decays at LEP*, Phys. Lett. B **371** (1996) 126.

[15] OPAL Collaboration, *Production of* $f_0(980)$, $f_2(1270)$ *and* $\phi(1020)$ *in hadronic* Z^0 *decay*, Euro. Phys. J. C **4** (1998) 19.

[16] T. Sjöstrand, Comp. Phys. Comm. **82** (1994) 74; preprint CERN-TH.7112/93 (1993, revised August 1994).

[17] G. Marchesini et al., Comp. Phys. Comm. **67** (1992) 465.

[18] L. Lönnblad, Comp. Phys. Comm. **71** (1992) 15.

[19] ALEPH Collaboration, *ALEPH: a detector for electron-positron annihilations at LEP*, Nucl. Instr. Meth. A **294** (1990) 121.

[20] ALEPH Collaboration, *Performance of the ALEPH detector at LEP*, Nucl. Instr. Meth. A **360** (1995) 481.

[21] ALEPH Collaboration, *Determination of the number of light neutrino species*, Phys. Lett. B **231** (1989) 519.

[22] *Report on hard QCD working group*, in Proc. Durham workshop on jet studies at LEP and HERA, J. Phys. G **17** (1991) 1537.
S. Catani et al., Phys. Lett. B **269** (1991) 432.
N. Brown and W.J. Stirling, Z. Phys. C **53** (1992) 629.

[23] J.E. Campagne and R. Zitoun, Z. Phys. C **43** (1989) 469.

[24] ALEPH Collaboration, *Production of* K^0 *and* Λ *in hadronic* Z *decays*, Z. Phys. C **64** (1994) 361.

[25] ALEPH Collaboration, *Studies of Quantum Chromodynamics with the ALEPH detector*, Phys. Rep. **294** (1998) 1.

[26] ALEPH Collaboration, *A measurement of the semileptonic branching ratio BR(*b-baryon $\rightarrow$ p$l\bar{\nu}X$*) and a study of inclusive* $\pi^{\pm}$, $K^{\pm}$, *(*p, $\overline{\mathrm{p}}$*) production in* Z *decays*, Euro. Phys. J. C **5** (1998) 205.

Table 1: Multiplicity for π^0 in different event types, compared with JETSET 7.4 and HERWIG 5.8 predictions. JETSET and HERWIG values for all x range are also given.

Event type		x range	Mult. $\pm \Delta_{\rm stat} \pm \Delta_{\rm syst}$	JETSET		HERWIG	
					all		all
Hadronic events		0.06 – 0.62	$2.131 \pm 0.007 \pm 0.079$	2.274	9.66	2.192	9.58
Two-jet events		0.06 – 0.52	$2.156 \pm 0.008 \pm 0.079$	2.313	8.54	2.169	8.54
Three-jet events	total	0.06 – 0.52	$2.069 \pm 0.011 \pm 0.097$	2.208	11.20	2.215	11.09
	jet 1	0.06 – 0.52	$0.978 \pm 0.008 \pm 0.056$	1.060	4.13	1.008	4.09
	jet 2	0.06 – 0.52	$0.790 \pm 0.007 \pm 0.030$	0.829	3.83	0.834	3.75
	jet 3	0.06 – 0.32	$0.301 \pm 0.003 \pm 0.011$	0.318	3.23	0.373	3.24

Table 2: Systematic and statistical errors for π^0. All values are expressed in percent.

Source of error	Hadronic events	Two-jet events	Three-jet events		
			Jet 1	Jet 2	Jet 3
Cut variations	2.9	3.0	3.0	2.6	1.9
Fit range	0.6	0.2	4.4	1.4	0.7
Energy calibration	2.2	2.0	2.1	2.3	3.1
Systematic error (quadrature total)	3.7	3.7	5.7	3.7	3.7
Statistical error	0.3	0.4	0.9	0.9	1.1

Table 3: Multiplicity for η in different event types, compared with JETSET 7.4 and HERWIG 5.8 predictions. JETSET and HERWIG values for all x range are also given.

Event type		x range	Mult. $\pm \Delta_{\mathrm{stat}} \pm \Delta_{\mathrm{syst}}$	JETSET		HERWIG	
					all		all
Hadronic events		0.10 – 1.0	$0.282 \pm 0.006 \pm 0.015$	0.297	1.03	0.331	0.98
Two-jet events		0.10 – 1.0	$0.280 \pm 0.007 \pm 0.020$	0.304	0.90	0.342	0.88
Three-jet events	total	0.10 – 0.62	$0.277 \pm 0.013 \pm 0.029$	0.283	1.20	0.317	1.12
	jet 1	0.10 – 0.62	$0.123 \pm 0.009 \pm 0.010$	0.138	0.432	0.155	0.421
	jet 2	0.10 – 0.52	$0.114 \pm 0.009 \pm 0.015$	0.108	0.402	0.121	0.382
	jet 3	0.10 – 0.32	$0.041 \pm 0.004 \pm 0.004$	0.037	0.366	0.041	0.320

Table 4: Systematic and statistical errors for η. All values are expressed in percent.

Source of error	Hadronic events	Two-jet events	Three-jet events		
			Jet 1	Jet 2	Jet 3
Cut variations	4.2	6.2	7.4	12.9	6.1
Fit range	1.5	2.4	3.3	2.6	5.7
Energy calibration	2.7	2.5	2.6	3.0	4.1
Systematic error (quadrature total)	5.3	7.1	8.5	13.5	9.3
Statistical error	2.2	2.4	6.9	7.6	9.5

Table 5: Multiplicity for $\eta'(958)$ in different event types, compared with JETSET 7.4 and HERWIG 5.8 predictions. JETSET and HERWIG values for all x range are also given.

Event type		x range	Mult. $\pm \Delta_{\rm stat} \pm \Delta_{\rm syst}$	JETSET		HERWIG	
					all		all
Hadronic events		0.16 – 1.0	0.045 $\pm$ 0.007 $\pm$ 0.007	0.045	0.155	0.054	0.131
Two-jet events		0.16 – 1.0	0.040 $\pm$ 0.006 $\pm$ 0.007	0.048	0.138	0.059	0.124
Three-jet events	total	0.16 – 0.52	0.039 $\pm$ 0.009 $\pm$ 0.009	0.038	0.180	0.046	0.142
	jet 1	0.16 – 0.52	0.019 $\pm$ 0.006 $\pm$ 0.004	0.020	0.066	0.025	0.059
	jet 2	0.16 – 0.52	0.016 $\pm$ 0.006 $\pm$ 0.004	0.015	0.060	0.018	0.051
	jet 3	0.16 – 0.34	0.0040 $\pm$ 0.0018 $\pm$ 0.0007	0.0034	0.053	0.0030	0.033

Table 6: Systematic and statistical errors for $\eta'(958)$. All values are expressed in percent.

Source of error	Hadronic events	Two-jet events	Three-jet events		
			Jet 1	Jet 2	Jet 3
η selection	5.0	6.7	7.8	13.2	7.3
$\pi^{\pm}$ selection	0.5	0.5	0.4	0.6	0.8
Fit range	14.4	15.7	21.9	20.4	17.0
Systematic error (quadrature total)	15.3	17.0	23.3	24.4	18.5
Statistical error	15.2	14.1	33.5	37.3	45.8

Table 7: Multiplicity for K^0 (K^0_S+K^0_L) in different event types, compared with JETSET 7.4, ARIADNE 4.08 and HERWIG 5.8 predictions. The extrapolation to the full ξ range is made using JETSET 7.4.

Event type		Mult. $\pm \Delta_{\rm stat} \pm \Delta_{\rm syst}$	JETSET	ARIADNE	HERWIG
Hadronic events		$2.093 \pm 0.004 \pm 0.016$	2.073	2.072	1.997
Two-jet events		$1.854 \pm 0.005 \pm 0.010$	1.865	1.872	1.892
Three-jet events	total	$2.394 \pm 0.008 \pm 0.035$	2.356	2.359	2.142
	jet 1	$0.884 \pm 0.005 \pm 0.012$	0.885	0.899	0.880
	jet 2	$0.826 \pm 0.004 \pm 0.014$	0.811	0.808	0.748
	jet 3	$0.684 \pm 0.004 \pm 0.009$	0.660	0.652	0.514

Table 8: Systematic and statistical errors for K^0_S. All values are expressed in percent.

Source of error	Hadronic events	Two-jet events	Three-jet events		
			Jet 1	Jet 2	Jet 3
$\mathrm{d}E/\mathrm{d}x$	0.11	0.25	0.3	0.4	0.4
$\chi^2_{\rm vertex\,fit}$	0.63	0.41	1.0	1.5	1.1
decay length	0.41	0.24	0.8	0.9	0.6
Systematic error (quadrature total)	0.76	0.54	1.3	1.7	1.3
Statistical error	0.19	0.27	0.48	0.56	0.58

Table 9: Multiplicity for Λ in different event types, compared with JETSET 7.4, ARIADNE 4.08 and HERWIG 5.8 predictions. The extrapolation to the full ξ range is made using JETSET 7.4.

Event type		Mult. $\pm \Delta_{\mathrm{stat}} \pm \Delta_{\mathrm{syst}}$	JETSET	ARIADNE	HERWIG
Hadronic events		$0.404 \pm 0.002 \pm 0.002$	0.397	0.401	0.466
Two-jet events		$0.350 \pm 0.003 \pm 0.002$	0.343	0.350	0.432
Three-jet events	total	$0.484 \pm 0.005 \pm 0.020$	0.470	0.477	0.516
	jet 1	$0.171 \pm 0.003 \pm 0.005$	0.163	0.170	0.202
	jet 2	$0.160 \pm 0.003 \pm 0.008$	0.152	0.152	0.172
	jet 3	$0.153 \pm 0.003 \pm 0.007$	0.155	0.155	0.142

Table 10: Systematic and statistical errors for Λ. All values are expressed in percent.

Source of error	Hadronic events	Two-jet events	Three-jet events		
			Jet 1	Jet 2	Jet 3
$\mathrm{d}E/\mathrm{d}x$	0.2	0.2	2.4	4.2	3.6
$\chi^2_{\text{vertex fit}}$	0.4	0.3	1.2	1.3	2.5
$\cos\theta^*$	0.1	0.4	1.1	2.2	1.3
Systematic error (quadrature total)	0.5	0.6	2.9	4.9	4.5
Statistical error	0.5	0.7	1.5	1.9	2.0

Table 11: Inclusive cross section for π^0 in hadronic events.

x range	$\frac{1}{\sigma_{\rm had}}\frac{{\rm d}\sigma(\pi^0)}{{\rm d}x} \pm \Delta_{\rm stat} \pm \Delta_{\rm syst}$
0.06 – 0.08	30.82 ± 0.25 ± 0.99
0.08 – 0.10	20.02 ± 0.13 ± 0.66
0.10 – 0.14	11.65 ± 0.05 ± 0.42
0.14 – 0.18	6.247 ± 0.029 ± 0.256
0.18 – 0.22	3.613 ± 0.018 ± 0.160
0.22 – 0.26	2.243 ± 0.013 ± 0.085
0.26 – 0.30	1.395 ± 0.013 ± 0.047
0.30 – 0.34	0.928 ± 0.012 ± 0.027
0.34 – 0.38	0.620 ± 0.011 ± 0.033
0.38 – 0.42	0.411 ± 0.011 ± 0.030
0.42 – 0.46	0.281 ± 0.013 ± 0.035
0.46 – 0.52	0.181 ± 0.015 ± 0.027
0.52 – 0.62	0.082 ± 0.015 ± 0.019

Table 12: Inclusive cross section for η in hadronic events.

x range	$\frac{1}{\sigma_{\rm had}}\frac{{\rm d}\sigma(\eta)}{{\rm d}x} \pm \Delta_{\rm stat} \pm \Delta_{\rm syst}$
0.10 – 0.14	2.07 ± 0.13 ± 0.14
0.14 – 0.18	1.379 ± 0.068 ± 0.074
0.18 – 0.22	0.917 ± 0.039 ± 0.050
0.22 – 0.26	0.704 ± 0.028 ± 0.025
0.26 – 0.30	0.492 ± 0.021 ± 0.019
0.30 – 0.34	0.379 ± 0.016 ± 0.012
0.34 – 0.38	0.265 ± 0.011 ± 0.014
0.38 – 0.42	0.205 ± 0.008 ± 0.010
0.42 – 0.46	0.168 ± 0.008 ± 0.010
0.46 – 0.50	0.120 ± 0.006 ± 0.007
0.50 – 0.54	0.0946 ± 0.0053 ± 0.0056
0.54 – 0.58	0.0747 ± 0.0041 ± 0.0036
0.58 – 0.62	0.0519 ± 0.0032 ± 0.0039
0.62 – 0.66	0.0371 ± 0.0025 ± 0.0017
0.66 – 0.70	0.0296 ± 0.0023 ± 0.0018
0.70 – 0.74	0.0211 ± 0.0018 ± 0.0020
0.74 – 0.82	0.0104 ± 0.0008 ± 0.0010
0.82 – 1.00	0.0015 ± 0.0002 ± 0.0001

Table 13: Inclusive cross section for $\eta'(958)$ in hadronic events.

x range	$\frac{1}{\sigma_{\rm had}}\frac{{\rm d}\sigma(\eta')}{{\rm d}x} \pm \Delta_{\rm stat} \pm \Delta_{\rm syst}$
0.16 – 0.26	0.210 ± 0.065 ± 0.032
0.26 – 0.34	0.132 ± 0.022 ± 0.020
0.34 – 0.40	0.082 ± 0.015 ± 0.012
0.40 – 0.46	0.036 ± 0.006 ± 0.005
0.46 – 0.52	0.035 ± 0.005 ± 0.005
0.52 – 0.58	0.023 ± 0.004 ± 0.004
0.58 – 0.64	0.0157 ± 0.0026 ± 0.0024
0.64 – 0.72	0.0107 ± 0.0015 ± 0.0016
0.72 – 0.80	0.0055 ± 0.0011 ± 0.0008
0.80 – 1.00	0.0011 ± 0.0002 ± 0.0002

Table 14: Inclusive cross section for π^0 in two-jet events.

x range	$\frac{1}{\sigma_2}\frac{\mathrm{d}\sigma(\pi^0)}{\mathrm{d}x} \pm \Delta_{\mathrm{stat}} \pm \Delta_{\mathrm{syst}}$
0.06 – 0.08	29.32 ± 0.30 ± 0.93
0.08 – 0.10	19.64 ± 0.16 ± 0.69
0.10 – 0.14	11.79 ± 0.07 ± 0.41
0.14 – 0.18	6.616 ± 0.036 ± 0.283
0.18 – 0.22	3.977 ± 0.023 ± 0.185
0.22 – 0.32	1.894 ± 0.011 ± 0.061
0.32 – 0.42	0.670 ± 0.010 ± 0.031
0.42 – 0.52	0.257 ± 0.013 ± 0.029

Table 15: Inclusive cross section for η in two-jet events.

x range	$\frac{1}{\sigma_2}\frac{\mathrm{d}\sigma(\eta)}{\mathrm{d}x} \pm \Delta_{\mathrm{stat}} \pm \Delta_{\mathrm{syst}}$
0.10 – 0.14	1.74 ± 0.13 ± 0.24
0.14 – 0.18	1.352 ± 0.073 ± 0.081
0.18 – 0.22	0.950 ± 0.045 ± 0.060
0.22 – 0.32	0.594 ± 0.016 ± 0.023
0.32 – 0.42	0.280 ± 0.007 ± 0.014
0.42 – 0.52	0.163 ± 0.005 ± 0.010
0.52 – 0.62	0.0844 ± 0.0027 ± 0.0045
0.62 – 0.72	0.0404 ± 0.0017 ± 0.0016
0.72 – 0.82	0.0164 ± 0.0010 ± 0.0011
0.82 – 1.00	0.0021 ± 0.0003 ± 0.0002

Table 16: Inclusive cross section for $\eta'(958)$ in two-jet events.

x range	$\frac{1}{\sigma_2}\frac{\mathrm{d}\sigma(\eta')}{\mathrm{d}x} \pm \Delta_{\mathrm{stat}} \pm \Delta_{\mathrm{syst}}$
0.16 – 0.26	0.145 ± 0.048 ± 0.025
0.26 – 0.34	0.136 ± 0.031 ± 0.023
0.34 – 0.42	0.084 ± 0.019 ± 0.014
0.42 – 0.52	0.032 ± 0.005 ± 0.005
0.52 – 0.62	0.023 ± 0.003 ± 0.004
0.62 – 0.72	0.0153 ± 0.0022 ± 0.0026
0.72 – 0.82	0.0074 ± 0.0013 ± 0.0013
0.82 – 1.00	0.0012 ± 0.0004 ± 0.0002

Table 17: Inclusive cross section for π^0 in three-jet events.

	x range	$\frac{1}{\sigma_3}\frac{\mathrm{d}\sigma(\pi^0)}{\mathrm{d}x}$	$\pm\ \Delta_{\mathrm{stat}}$	$\pm\ \Delta_{\mathrm{syst}}$
Jet 1	0.06 – 0.08	13.14	± 0.32	± 0.72
	0.08 – 0.10	9.13	± 0.18	± 0.47
	0.10 – 0.14	5.57	± 0.06	± 0.34
	0.14 – 0.18	3.024	± 0.035	± 0.175
	0.18 – 0.22	1.712	± 0.025	± 0.109
	0.22 – 0.32	0.792	± 0.011	± 0.045
	0.32 – 0.42	0.294	± 0.011	± 0.019
	0.42 – 0.52	0.116	± 0.021	± 0.019
Jet 2	0.06 – 0.08	12.80	± 0.28	± 0.50
	0.08 – 0.10	8.05	± 0.14	± 0.29
	0.10 – 0.14	4.402	± 0.046	± 0.151
	0.14 – 0.18	2.214	± 0.028	± 0.087
	0.18 – 0.22	1.129	± 0.018	± 0.037
	0.22 – 0.32	0.4593	± 0.0069	± 0.0175
	0.32 – 0.42	0.1271	± 0.0051	± 0.0040
	0.42 – 0.52	0.0414	± 0.0075	± 0.0094
Jet 3	0.06 – 0.08	6.69	± 0.14	± 0.24
	0.08 – 0.10	3.622	± 0.060	± 0.154
	0.10 – 0.14	1.496	± 0.019	± 0.052
	0.14 – 0.18	0.5171	± 0.0094	± 0.0195
	0.18 – 0.22	0.2041	± 0.0054	± 0.0080
	0.22 – 0.32	0.0588	± 0.0019	± 0.0025

Table 18: Inclusive cross section for η in three-jet events.

	x range	$\frac{1}{\sigma_3}\frac{\mathrm{d}\sigma(\eta)}{\mathrm{d}x} \pm \Delta_{\mathrm{stat}} \pm \Delta_{\mathrm{syst}}$
Jet 1	0.10 – 0.14	0.849 ± 0.182 ± 0.095
	0.14 – 0.18	0.644 ± 0.088 ± 0.058
	0.18 – 0.22	0.338 ± 0.039 ± 0.036
	0.22 – 0.32	0.257 ± 0.018 ± 0.015
	0.32 – 0.42	0.1382 ± 0.0095 ± 0.0075
	0.42 – 0.52	0.0650 ± 0.0054 ± 0.0060
	0.52 – 0.62	0.0325 ± 0.0031 ± 0.0018
Jet 2	0.10 – 0.14	1.09 ± 0.19 ± 0.25
	0.14 – 0.18	0.629 ± 0.083 ± 0.057
	0.18 – 0.22	0.349 ± 0.038 ± 0.020
	0.22 – 0.32	0.197 ± 0.013 ± 0.018
	0.32 – 0.42	0.0848 ± 0.0060 ± 0.0048
	0.42 – 0.52	0.0303 ± 0.0030 ± 0.0030
Jet 3	0.10 – 0.14	0.584 ± 0.092 ± 0.056
	0.14 – 0.18	0.240 ± 0.030 ± 0.019
	0.18 – 0.22	0.118 ± 0.014 ± 0.013
	0.22 – 0.32	0.0344 ± 0.0034 ± 0.0035

Table 19: Inclusive cross section for $\eta'(958)$ in three-jet events.

	x range	$\frac{1}{\sigma_3}\frac{\mathrm{d}\sigma(\eta')}{\mathrm{d}x} \pm \Delta_{\mathrm{stat}} \pm \Delta_{\mathrm{syst}}$
Jet 1	0.16 – 0.26	0.101 ± 0.058 ± 0.024
	0.26 – 0.34	0.044 ± 0.023 ± 0.010
	0.34 – 0.42	0.037 ± 0.013 ± 0.009
	0.42 – 0.52	0.0193 ± 0.0045 ± 0.0045
Jet 2	0.16 – 0.26	0.090 ± 0.059 ± 0.022
	0.26 – 0.34	0.049 ± 0.016 ± 0.012
	0.34 – 0.42	0.0235 ± 0.0071 ± 0.0057
	0.42 – 0.52	0.0156 ± 0.0039 ± 0.0038
Jet 3	0.16 – 0.26	0.033 ± 0.018 ± 0.006
	0.26 – 0.34	0.0086 ± 0.0035 ± 0.0016

Table 20: Inclusive cross section for K^0_S in hadronic events.

ξ range	$\frac{1}{\sigma_{\rm had}}\frac{d\sigma(K^0_S)}{d\xi} \pm \Delta_{\rm stat} \pm \Delta_{\rm syst}$
0.2 – 0.4	0.018 ± 0.002 ± 0.005
0.4 – 0.6	0.035 ± 0.002 ± 0.006
0.6 – 0.8	0.066 ± 0.003 ± 0.006
0.8 – 1.0	0.096 ± 0.002 ± 0.004
1.0 – 1.2	0.147 ± 0.002 ± 0.002
1.2 – 1.4	0.193 ± 0.002 ± 0.003
1.4 – 1.6	0.233 ± 0.002 ± 0.004
1.6 – 1.8	0.273 ± 0.002 ± 0.005
1.8 – 2.0	0.306 ± 0.002 ± 0.005
2.0 – 2.2	0.326 ± 0.002 ± 0.005
2.2 – 2.4	0.339 ± 0.002 ± 0.005
2.4 – 2.6	0.349 ± 0.002 ± 0.004
2.6 – 2.8	0.348 ± 0.002 ± 0.003
2.8 – 3.0	0.339 ± 0.002 ± 0.003
3.0 – 3.2	0.326 ± 0.002 ± 0.003
3.2 – 3.4	0.312 ± 0.002 ± 0.003
3.4 – 3.6	0.291 ± 0.002 ± 0.003
3.6 – 3.8	0.265 ± 0.002 ± 0.003
3.8 – 4.0	0.235 ± 0.002 ± 0.003
4.0 – 4.2	0.200 ± 0.002 ± 0.003
4.2 – 4.4	0.160 ± 0.002 ± 0.003
4.4 – 4.6	0.122 ± 0.002 ± 0.002
4.6 – 4.8	0.090 ± 0.003 ± 0.002

Table 21: Inclusive cross section for Λ in hadronic events.

ξ range	$\frac{1}{\sigma_{\rm had}}\frac{d\sigma(\Lambda)}{d\xi} \pm \Delta_{\rm stat} \pm \Delta_{\rm syst}$
0.4 – 0.6	0.016 ± 0.001 ± 0.001
0.6 – 0.8	0.031 ± 0.001 ± 0.001
0.8 – 1.0	0.053 ± 0.002 ± 0.001
1.0 – 1.2	0.066 ± 0.002 ± 0.001
1.2 – 1.4	0.083 ± 0.002 ± 0.001
1.4 – 1.6	0.099 ± 0.002 ± 0.001
1.6 – 1.8	0.111 ± 0.003 ± 0.001
1.8 – 2.0	0.123 ± 0.003 ± 0.001
2.0 – 2.2	0.130 ± 0.003 ± 0.001
2.2 – 2.4	0.135 ± 0.002 ± 0.001
2.4 – 2.6	0.141 ± 0.002 ± 0.002
2.6 – 2.8	0.145 ± 0.003 ± 0.002
2.8 – 3.0	0.145 ± 0.003 ± 0.003
3.0 – 3.2	0.143 ± 0.003 ± 0.004
3.2 – 3.4	0.126 ± 0.003 ± 0.004
3.4 – 3.6	0.114 ± 0.003 ± 0.003
3.6 – 3.8	0.093 ± 0.002 ± 0.002
3.8 – 4.0	0.081 ± 0.002 ± 0.002
4.0 – 4.2	0.061 ± 0.002 ± 0.002
4.2 – 4.4	0.050 ± 0.003 ± 0.003
4.4 – 4.6	0.024 ± 0.003 ± 0.004
4.6 – 4.8	0.017 ± 0.003 ± 0.003

Table 22: Inclusive cross section for K^0_S in two-jet events.

ξ range	$\frac{1}{\sigma_2}\frac{d\sigma(K^0_S)}{d\xi} \pm \Delta_{stat} \pm \Delta_{syst}$
0.2 – 0.4	0.026 ± 0.003 ± 0.004
0.4 – 0.6	0.042 ± 0.003 ± 0.003
0.6 – 0.8	0.077 ± 0.003 ± 0.002
0.8 – 1.0	0.110 ± 0.003 ± 0.002
1.0 – 1.2	0.166 ± 0.003 ± 0.002
1.2 – 1.4	0.212 ± 0.002 ± 0.002
1.4 – 1.6	0.248 ± 0.002 ± 0.003
1.6 – 1.8	0.275 ± 0.002 ± 0.003
1.8 – 2.0	0.299 ± 0.002 ± 0.003
2.0 – 2.2	0.306 ± 0.002 ± 0.003
2.2 – 2.4	0.299 ± 0.002 ± 0.002
2.4 – 2.6	0.294 ± 0.002 ± 0.002
2.6 – 2.8	0.281 ± 0.002 ± 0.003
2.8 – 3.0	0.262 ± 0.002 ± 0.003
3.0 – 3.2	0.247 ± 0.002 ± 0.002
3.2 – 3.4	0.236 ± 0.002 ± 0.002
3.4 – 3.6	0.220 ± 0.002 ± 0.002
3.6 – 3.8	0.207 ± 0.002 ± 0.002
3.8 – 4.0	0.189 ± 0.002 ± 0.002
4.0 – 4.2	0.165 ± 0.002 ± 0.003
4.2 – 4.4	0.137 ± 0.003 ± 0.003
4.4 – 4.6	0.108 ± 0.003 ± 0.003
4.6 – 4.8	0.077 ± 0.003 ± 0.003

Table 23: Inclusive cross section for Λ in two-jet events.

ξ range	$\frac{1}{\sigma_2}\frac{d\sigma(\Lambda)}{d\xi} \pm \Delta_{stat} \pm \Delta_{syst}$
0.4 – 0.6	0.022 ± 0.002 ± 0.002
0.6 – 0.8	0.040 ± 0.002 ± 0.002
0.8 – 1.0	0.065 ± 0.002 ± 0.002
1.0 – 1.2	0.074 ± 0.002 ± 0.002
1.2 – 1.4	0.087 ± 0.003 ± 0.002
1.4 – 1.6	0.101 ± 0.003 ± 0.002
1.6 – 1.8	0.107 ± 0.003 ± 0.002
1.8 – 2.0	0.110 ± 0.003 ± 0.002
2.0 – 2.2	0.109 ± 0.003 ± 0.002
2.2 – 2.4	0.107 ± 0.003 ± 0.002
2.4 – 2.6	0.104 ± 0.003 ± 0.002
2.6 – 2.8	0.107 ± 0.002 ± 0.003
2.8 – 3.0	0.101 ± 0.002 ± 0.005
3.0 – 3.2	0.102 ± 0.003 ± 0.005
3.2 – 3.4	0.098 ± 0.003 ± 0.004
3.4 – 3.6	0.092 ± 0.003 ± 0.003
3.6 – 3.8	0.078 ± 0.003 ± 0.002
3.8 – 4.0	0.071 ± 0.002 ± 0.003
4.0 – 4.2	0.056 ± 0.003 ± 0.005
4.2 – 4.4	0.040 ± 0.003 ± 0.006
4.4 – 4.6	0.026 ± 0.004 ± 0.006
4.6 – 4.8	0.015 ± 0.003 ± 0.004

Table 24: Inclusive cross section for K^0_S in the first jet of three-jet events.

ξ range	$\frac{1}{\sigma_3}\frac{d\sigma(K^0_S)}{d\xi} \pm \Delta_{stat} \pm \Delta_{syst}$
0.6 – 0.8	0.030 ± 0.003 ± 0.005
0.8 – 1.0	0.045 ± 0.003 ± 0.004
1.0 – 1.2	0.074 ± 0.003 ± 0.004
1.2 – 1.4	0.096 ± 0.003 ± 0.005
1.4 – 1.6	0.112 ± 0.002 ± 0.005
1.6 – 1.8	0.131 ± 0.002 ± 0.004
1.8 – 2.0	0.143 ± 0.002 ± 0.002
2.0 – 2.2	0.147 ± 0.002 ± 0.002
2.2 – 2.4	0.148 ± 0.002 ± 0.002
2.4 – 2.6	0.149 ± 0.002 ± 0.002
2.6 – 2.8	0.140 ± 0.002 ± 0.002
2.8 – 3.0	0.136 ± 0.002 ± 0.002
3.0 – 3.2	0.128 ± 0.002 ± 0.002
3.2 – 3.4	0.120 ± 0.002 ± 0.002
3.4 – 3.6	0.110 ± 0.002 ± 0.002
3.6 – 3.8	0.100 ± 0.002 ± 0.002
3.8 – 4.0	0.090 ± 0.003 ± 0.002
4.0 – 4.2	0.077 ± 0.003 ± 0.003
4.2 – 4.4	0.062 ± 0.003 ± 0.003
4.4 – 4.6	0.050 ± 0.003 ± 0.003
4.6 – 4.8	0.037 ± 0.004 ± 0.002

Table 25: Inclusive cross section for K^0_S in the second jet of three-jet events.

ξ range	$\frac{1}{\sigma_3}\frac{d\sigma(K^0_S)}{d\xi} \pm \Delta_{stat} \pm \Delta_{syst}$
0.4 – 0.6	0.007 ± 0.001 ± 0.001
0.6 – 0.8	0.016 ± 0.002 ± 0.002
0.8 – 1.0	0.027 ± 0.002 ± 0.002
1.0 – 1.2	0.044 ± 0.002 ± 0.003
1.2 – 1.4	0.063 ± 0.002 ± 0.003
1.4 – 1.6	0.084 ± 0.002 ± 0.002
1.6 – 1.8	0.108 ± 0.002 ± 0.002
1.8 – 2.0	0.125 ± 0.002 ± 0.003
2.0 – 2.2	0.142 ± 0.002 ± 0.005
2.2 – 2.4	0.151 ± 0.002 ± 0.006
2.4 – 2.6	0.157 ± 0.002 ± 0.005
2.6 – 2.8	0.161 ± 0.002 ± 0.004
2.8 – 3.0	0.154 ± 0.002 ± 0.004
3.0 – 3.2	0.149 ± 0.002 ± 0.004
3.2 – 3.4	0.131 ± 0.002 ± 0.003
3.4 – 3.6	0.118 ± 0.002 ± 0.002
3.6 – 3.8	0.101 ± 0.003 ± 0.002
3.8 – 4.0	0.085 ± 0.003 ± 0.002
4.0 – 4.2	0.070 ± 0.003 ± 0.005
4.2 – 4.4	0.055 ± 0.003 ± 0.011
4.4 – 4.6	0.036 ± 0.003 ± 0.018
4.6 – 4.8	0.029 ± 0.003 ± 0.019

Table 26: Inclusive cross section for K^0_S in the third jet of three-jet events.

ξ range	$\frac{1}{\sigma_3}\frac{d\sigma(K^0_S)}{d\xi} \pm \Delta_{stat} \pm \Delta_{syst}$
0.8 – 1.0	0.0015 ± 0.0006 ± 0.0012
1.0 – 1.2	0.0042 ± 0.0005 ± 0.0006
1.2 – 1.4	0.0101 ± 0.0005 ± 0.0004
1.4 – 1.6	0.0175 ± 0.0006 ± 0.0003
1.6 – 1.8	0.0299 ± 0.0009 ± 0.0004
1.8 – 2.0	0.0504 ± 0.0011 ± 0.0006
2.0 – 2.2	0.068 ± 0.001 ± 0.001
2.2 – 2.4	0.093 ± 0.002 ± 0.002
2.4 – 2.6	0.113 ± 0.002 ± 0.003
2.6 – 2.8	0.135 ± 0.002 ± 0.004
2.8 – 3.0	0.152 ± 0.002 ± 0.003
3.0 – 3.2	0.155 ± 0.002 ± 0.003
3.2 – 3.4	0.158 ± 0.003 ± 0.003
3.4 – 3.6	0.149 ± 0.003 ± 0.003
3.6 – 3.8	0.139 ± 0.003 ± 0.002
3.8 – 4.0	0.116 ± 0.003 ± 0.002
4.0 – 4.2	0.097 ± 0.003 ± 0.002
4.2 – 4.4	0.072 ± 0.003 ± 0.002
4.4 – 4.6	0.053 ± 0.004 ± 0.002
4.6 – 4.8	0.036 ± 0.003 ± 0.002

Table 27: Inclusive cross section for Λ in the first jet of three-jet events.

ξ range	$\frac{1}{\sigma_3}\frac{d\sigma(\Lambda)}{d\xi} \pm \Delta_{stat} \pm \Delta_{syst}$
0.4 – 0.6	0.007 ± 0.002 ± 0.003
0.6 – 0.8	0.015 ± 0.002 ± 0.002
0.8 – 1.0	0.025 ± 0.002 ± 0.002
1.0 – 1.2	0.035 ± 0.003 ± 0.002
1.2 – 1.4	0.044 ± 0.003 ± 0.001
1.4 – 1.6	0.050 ± 0.004 ± 0.001
1.6 – 1.8	0.051 ± 0.004 ± 0.001
1.8 – 2.0	0.058 ± 0.004 ± 0.001
2.0 – 2.2	0.055 ± 0.003 ± 0.001
2.2 – 2.4	0.056 ± 0.003 ± 0.001
2.4 – 2.6	0.056 ± 0.003 ± 0.001
2.6 – 2.8	0.055 ± 0.003 ± 0.002
2.8 – 3.0	0.057 ± 0.003 ± 0.002
3.0 – 3.2	0.054 ± 0.003 ± 0.002
3.2 – 3.4	0.051 ± 0.003 ± 0.002
3.4 – 3.6	0.045 ± 0.003 ± 0.002
3.6 – 3.8	0.037 ± 0.002 ± 0.002
3.8 – 4.0	0.033 ± 0.003 ± 0.003
4.0 – 4.2	0.024 ± 0.003 ± 0.005
4.2 – 4.4	0.016 ± 0.004 ± 0.007

Table 28: Inclusive cross section for Λ in the second jet of three-jet events.

ξ range	$\frac{1}{\sigma_3}\frac{\mathrm{d}\sigma(\Lambda)}{\mathrm{d}\xi} \pm \Delta_{\mathrm{stat}} \pm \Delta_{\mathrm{syst}}$
0.6 – 0.8	0.006 ± 0.001 ± 0.004
0.8 – 1.0	0.013 ± 0.001 ± 0.003
1.0 – 1.2	0.023 ± 0.002 ± 0.002
1.2 – 1.4	0.032 ± 0.002 ± 0.001
1.4 – 1.6	0.041 ± 0.003 ± 0.001
1.6 – 1.8	0.051 ± 0.004 ± 0.001
1.8 – 2.0	0.061 ± 0.004 ± 0.002
2.0 – 2.2	0.066 ± 0.004 ± 0.002
2.2 – 2.4	0.073 ± 0.004 ± 0.002
2.4 – 2.6	0.072 ± 0.004 ± 0.002
2.6 – 2.8	0.069 ± 0.003 ± 0.001
2.8 – 3.0	0.064 ± 0.004 ± 0.001
3.0 – 3.2	0.059 ± 0.004 ± 0.002
3.2 – 3.4	0.046 ± 0.003 ± 0.002
3.4 – 3.6	0.035 ± 0.003 ± 0.003
3.6 – 3.8	0.030 ± 0.002 ± 0.004
3.8 – 4.0	0.018 ± 0.002 ± 0.005
4.0 – 4.2	0.015 ± 0.003 ± 0.006
4.2 – 4.4	0.008 ± 0.003 ± 0.006

Table 29: Inclusive cross section for Λ in the third jet of three-jet events.

ξ range	$\frac{1}{\sigma_3}\frac{\mathrm{d}\sigma(\Lambda)}{\mathrm{d}\xi} \pm \Delta_{\mathrm{stat}} \pm \Delta_{\mathrm{syst}}$
1.2 – 1.4	0.004 ± 0.001 ± 0.000
1.4 – 1.6	0.010 ± 0.002 ± 0.001
1.6 – 1.8	0.019 ± 0.002 ± 0.001
1.8 – 2.0	0.031 ± 0.002 ± 0.001
2.0 – 2.2	0.043 ± 0.003 ± 0.001
2.2 – 2.4	0.054 ± 0.003 ± 0.001
2.4 – 2.6	0.070 ± 0.003 ± 0.001
2.6 – 2.8	0.081 ± 0.004 ± 0.001
2.8 – 3.0	0.083 ± 0.004 ± 0.001
3.0 – 3.2	0.081 ± 0.004 ± 0.002
3.2 – 3.4	0.071 ± 0.003 ± 0.002
3.4 – 3.6	0.062 ± 0.003 ± 0.002
3.6 – 3.8	0.049 ± 0.003 ± 0.002
3.8 – 4.0	0.041 ± 0.003 ± 0.003
4.0 – 4.2	0.025 ± 0.003 ± 0.005

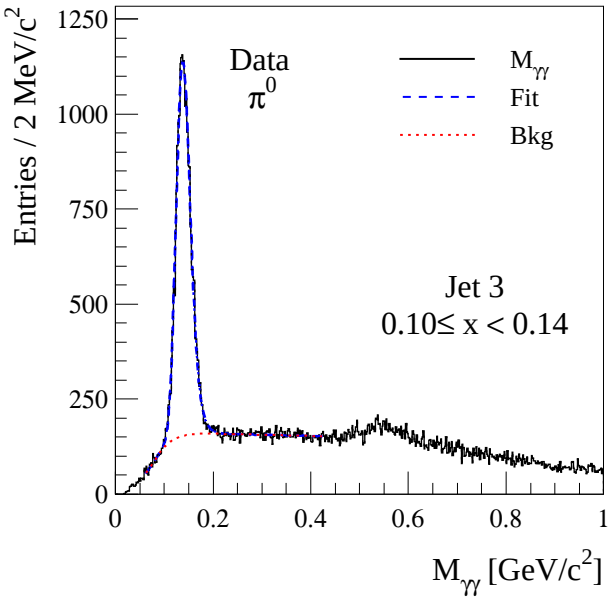

Figure 1: Example of a fitted $\gamma\gamma$ invariant mass distribution in jet 3 for inclusive π^0 production in three-jet events.

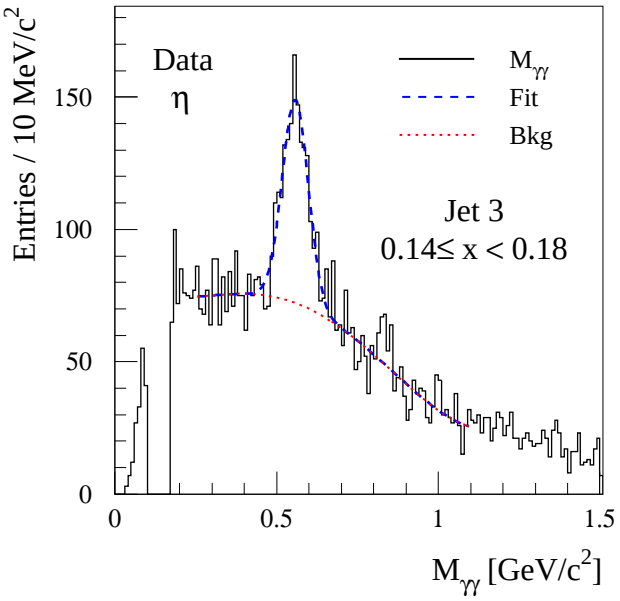

Figure 2: Example of a fitted $\gamma\gamma$ invariant mass distribution in jet 3 for inclusive η production in three-jet events.

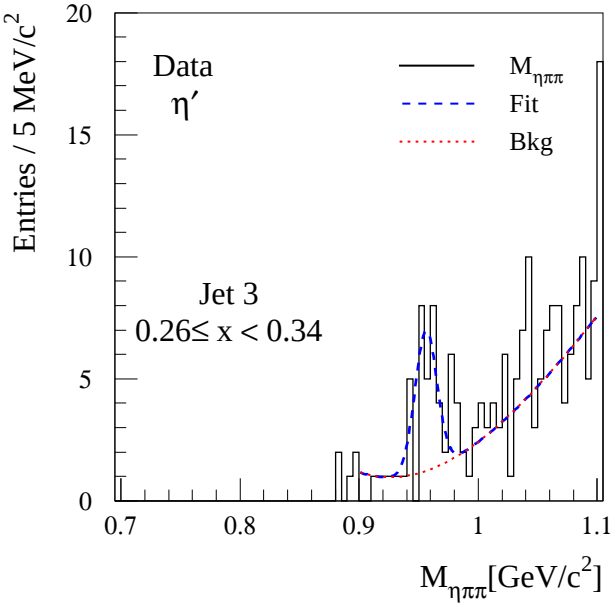

Figure 3: Example of a fitted $\eta\pi^+\pi^-$ invariant mass distribution in jet 3 for inclusive $\eta'(958)$ production in three-jet events.

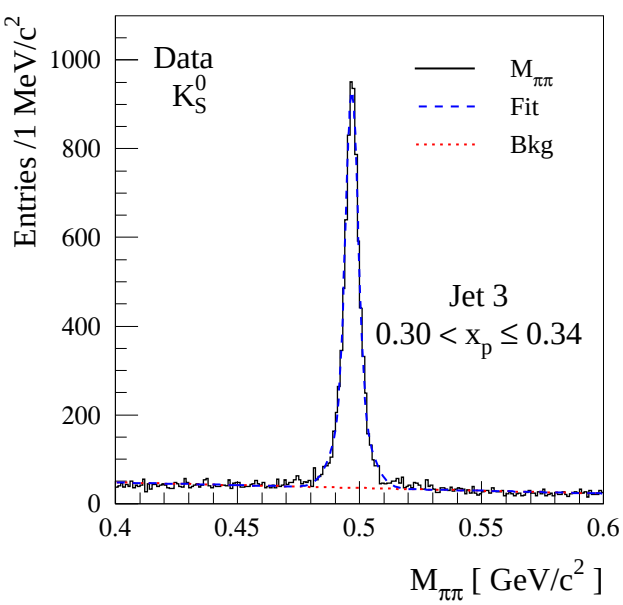

Figure 4: Example of a fitted $\pi^+\pi^-$ invariant mass distribution in jet 3 for inclusive K^0_S production in three-jet events.

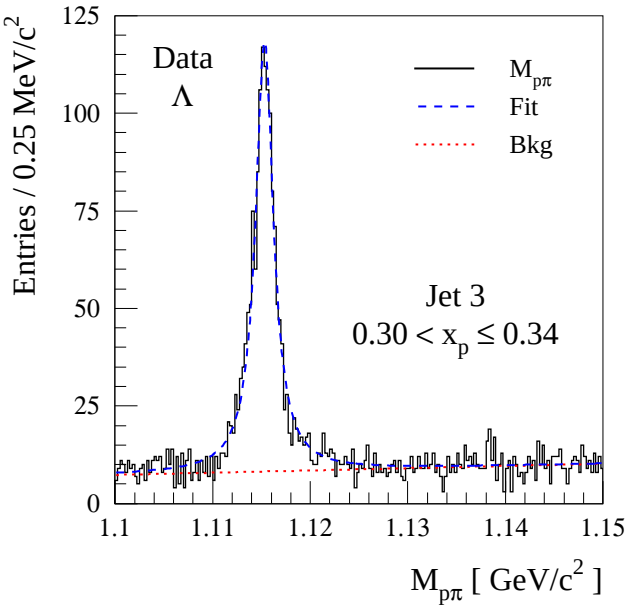

Figure 5: Example of a fitted $p\pi^-$ invariant mass distribution in jet 3 for inclusive Λ production in three-jet events.

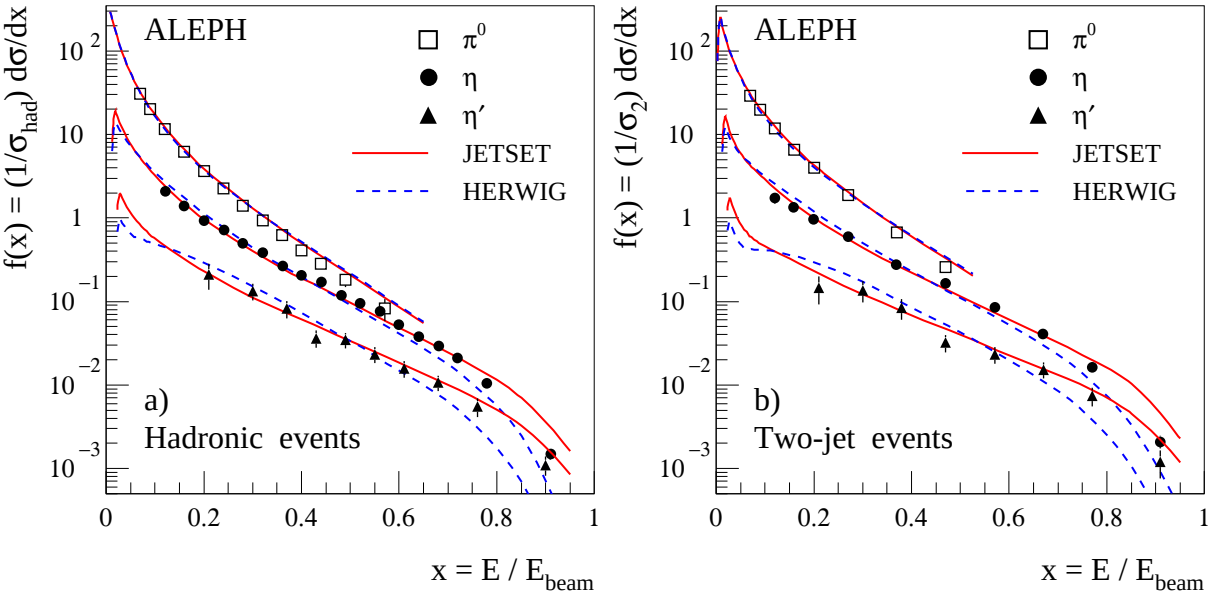

Figure 6: The inclusive cross sections of π^0, η, and $\eta'(958)$ in (a) all hadronic events and (b) two-jet events. The error bars show the total errors (statistical and systematic errors added in quadrature).

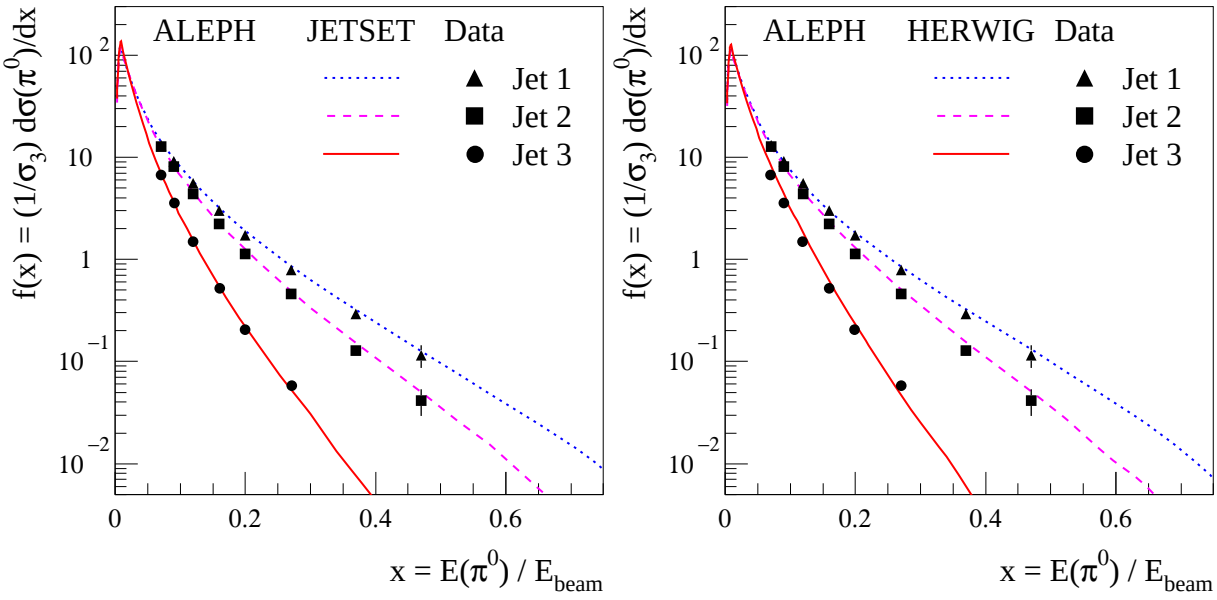

Figure 7: The inclusive cross sections of π^0 in three-jet events compared with JETSET 7.4 and HERWIG 5.8. The error bars show the total errors (statistical and systematic errors added in quadrature).

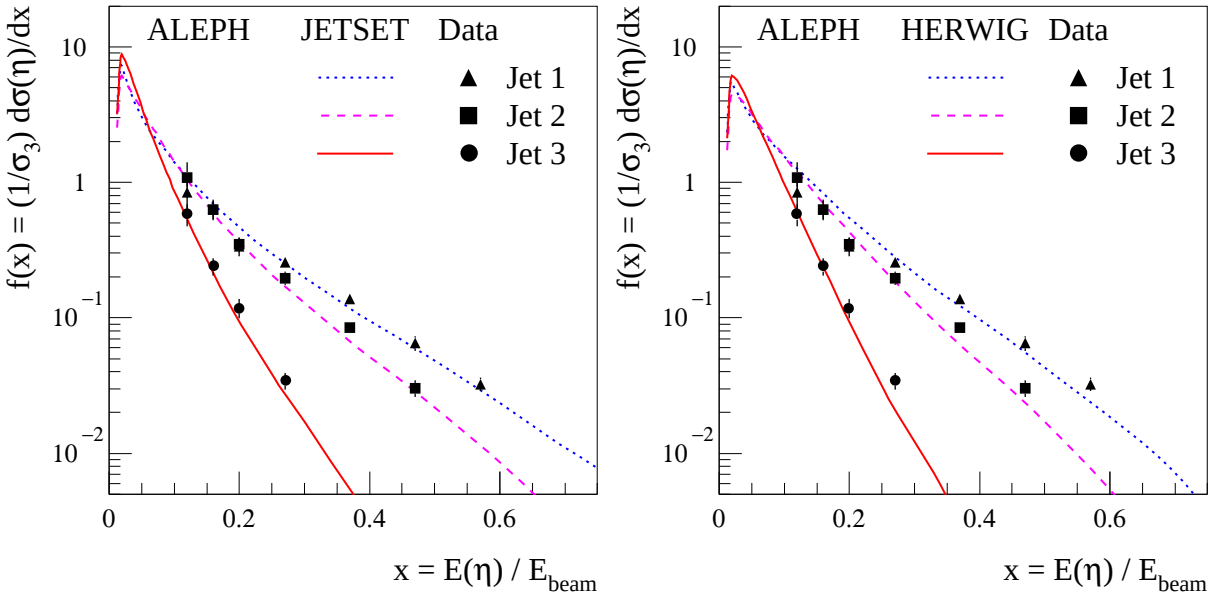

Figure 8: The inclusive cross sections of η in three-jet events compared with JETSET 7.4 and HERWIG 5.8. The error bars show the total errors (statistical and systematic errors added in quadrature).

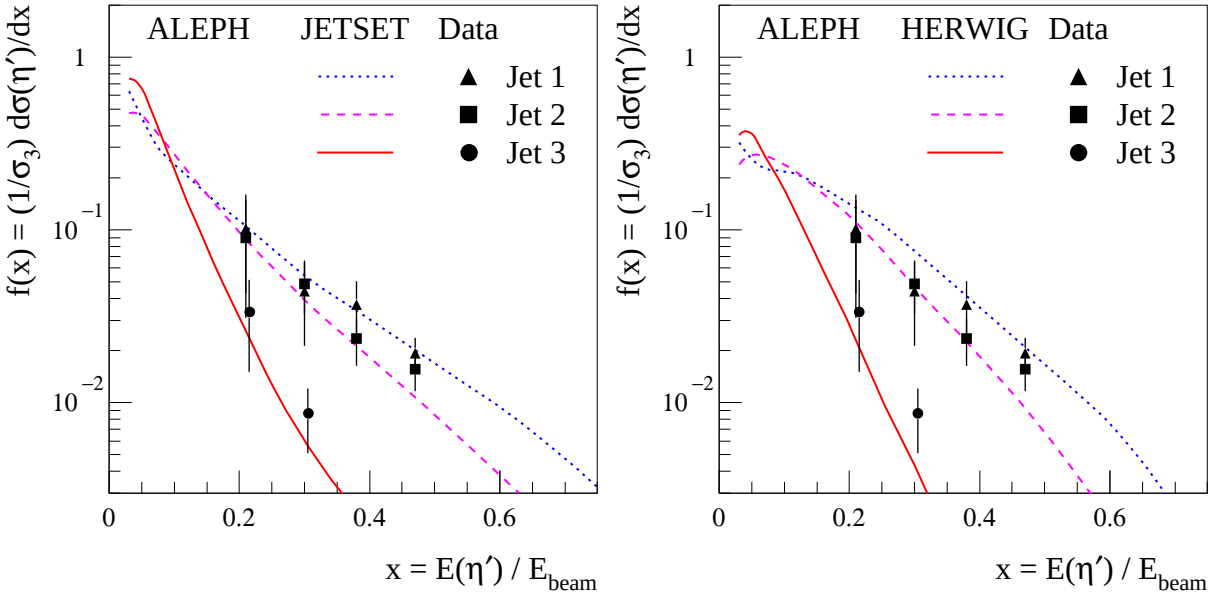

Figure 9: The inclusive cross sections of $\eta'(958)$ in three-jet events compared with JETSET 7.4 and HERWIG 5.8. The error bars show the statistical errors only.

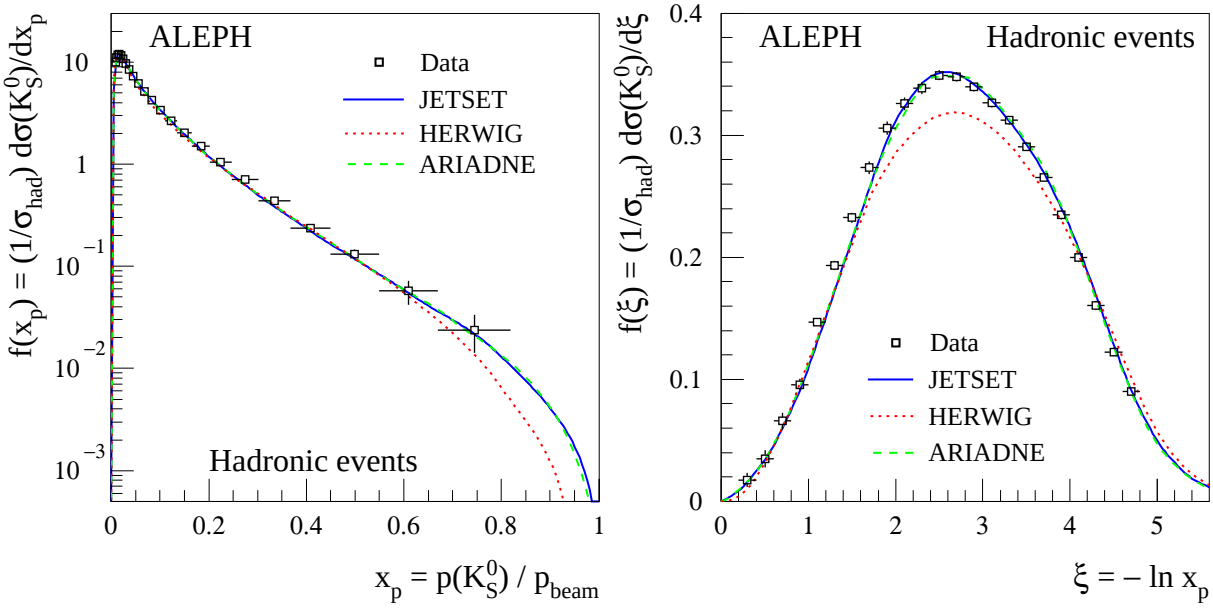

Figure 10: The inclusive cross sections of K^0_S in hadronic events in $x_p = p(\mathrm{K}^0_\mathrm{S})/p_\mathrm{beam}$ and $\xi = -\ln x_p$. The error bars show the total errors (statistical and systematic errors added in quadrature).

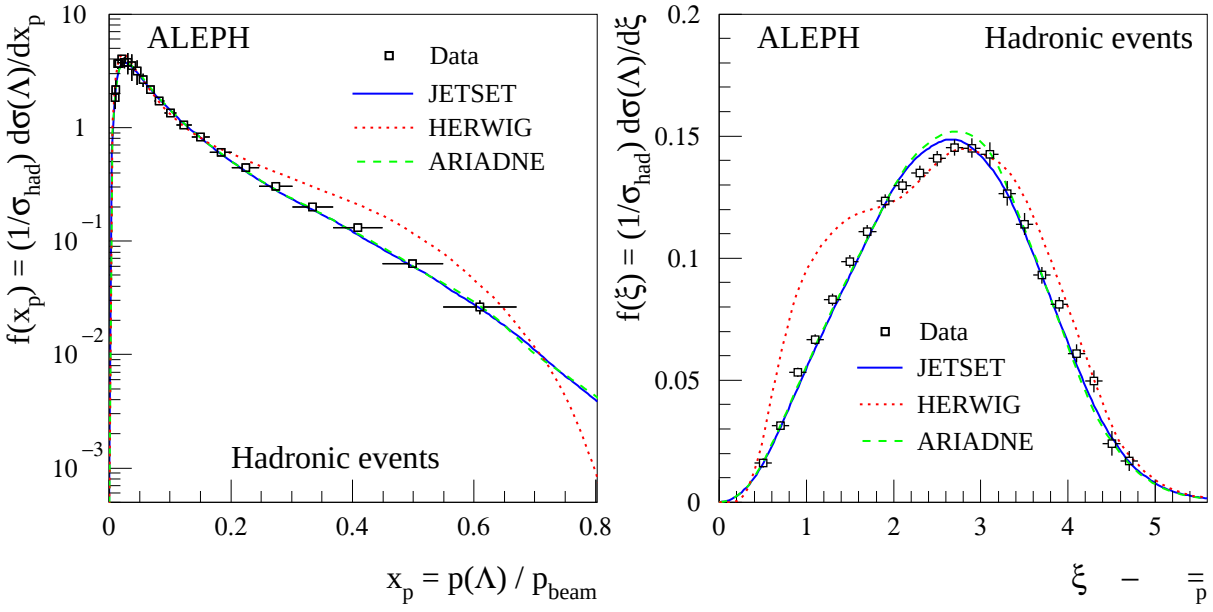

Figure 11: The inclusive cross sections of Λ and $\overline{\Lambda}$ in hadronic events in $x_p = p(\Lambda)/p_{\rm beam}$ and $\xi = -\ln x_p$. The error bars show the total errors (statistical and systematic errors added in quadrature).

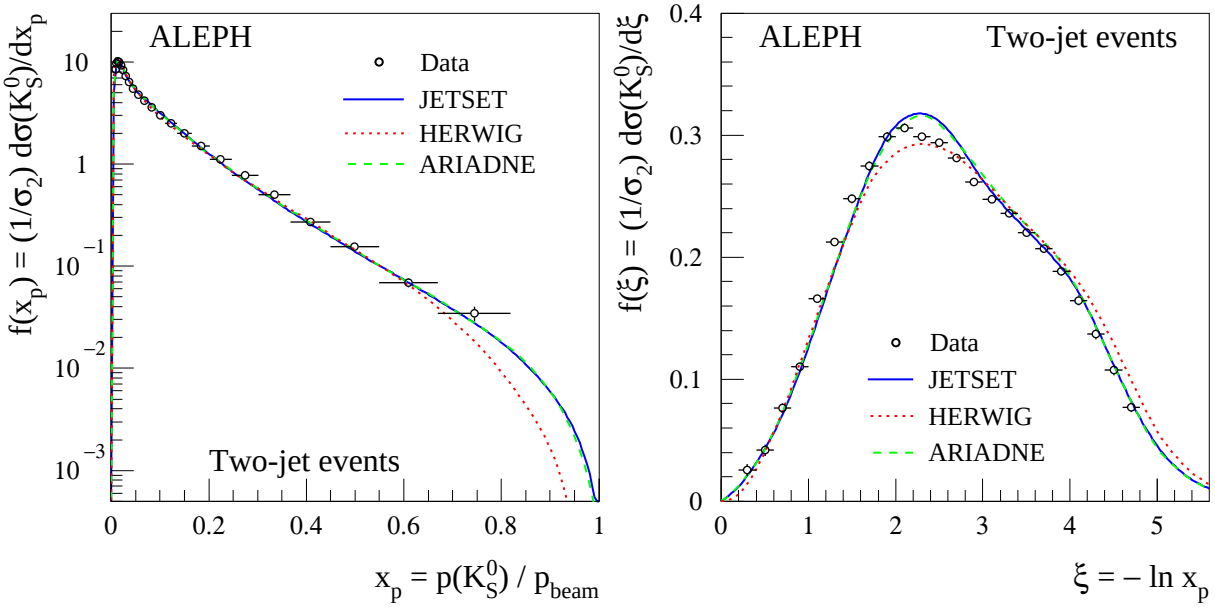

Figure 12: The inclusive cross sections of $\rm K^0_S$ in two-jet events in $x_p = p(\rm K^0_S)/p_{\rm beam}$ and $\xi = -\ln x_p$. The error bars show the total errors (statistical and systematic errors added in quadrature).

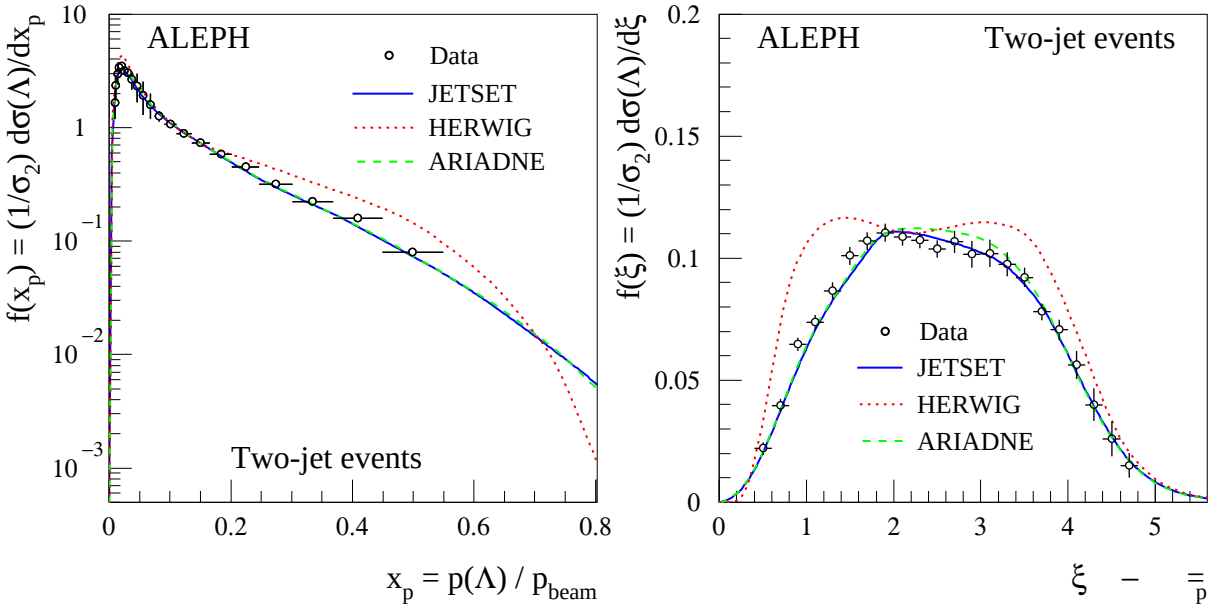

Figure 13: The inclusive cross sections of Λ and $\overline{\Lambda}$ in two-jet events in $x_p = p(\Lambda)/p_{\mathrm{beam}}$ and $\xi = -\ln x_p$. The error bars show the total errors (statistical and systematic errors added in quadrature).

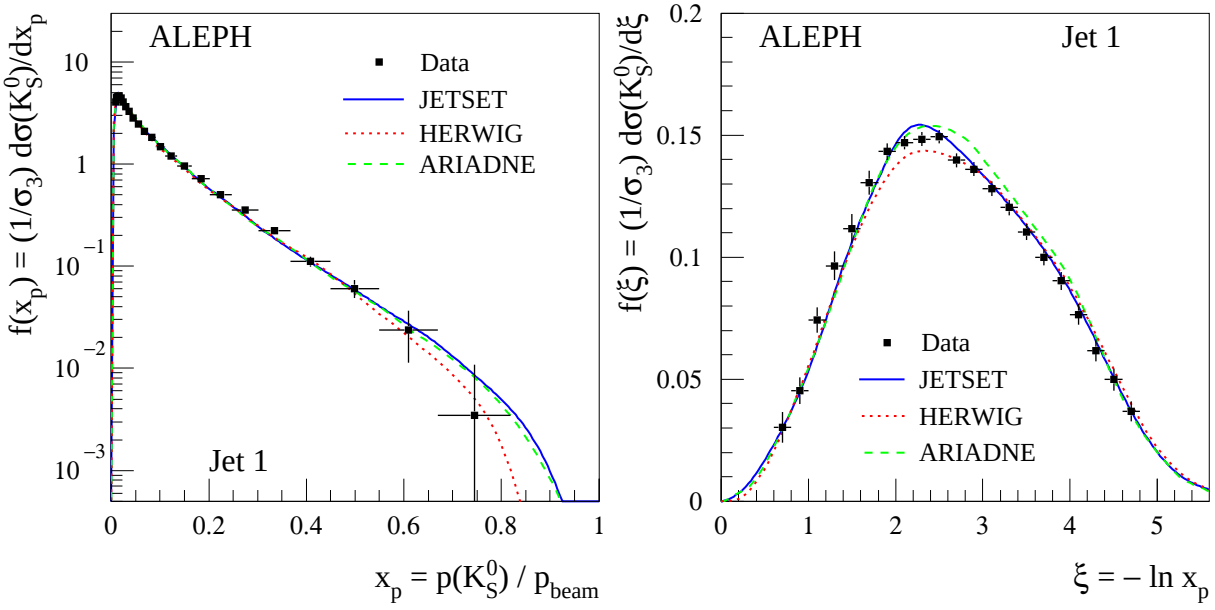

Figure 14: The inclusive cross sections of $\mathrm{K}^0_{\mathrm{S}}$ in the first jet of the three-jet events in $x_p = p(\mathrm{K}^0_{\mathrm{S}})/p_{\mathrm{beam}}$ and $\xi = -\ln x_p$. The error bars show the total errors (statistical and systematic errors added in quadrature).

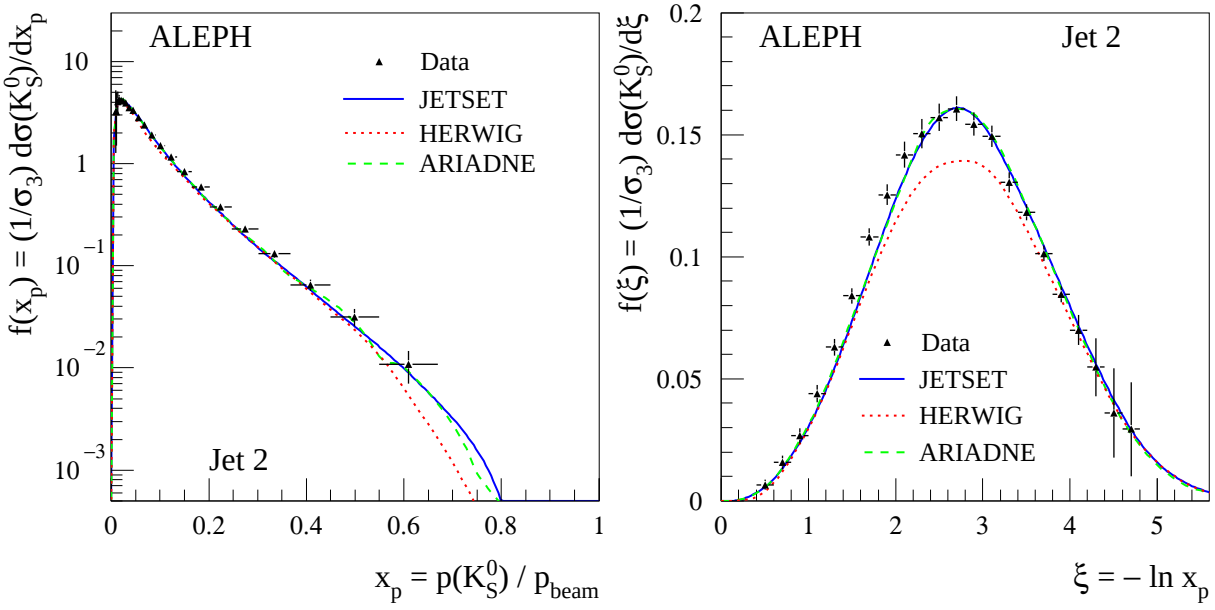

Figure 15: The inclusive cross sections of K^0_S in the second jet of the three-jet events in $x_p = p(K^0_S)/p_{beam}$ and $\xi = -\ln x_p$. The error bars show the total errors (statistical and systematic errors added in quadrature).

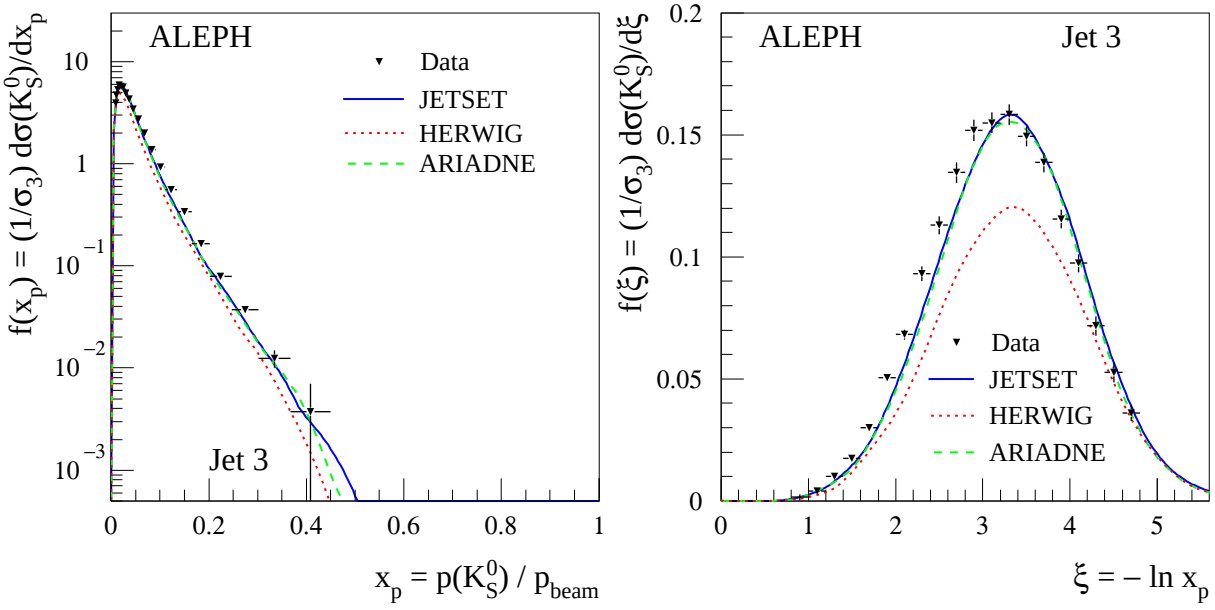

Figure 16: The inclusive cross sections of K^0_S in the third jet of the three-jet events in $x_p = p(K^0_S)/p_{beam}$ and $\xi = -\ln x_p$. The error bars show the total errors (statistical and systematic errors added in quadrature).

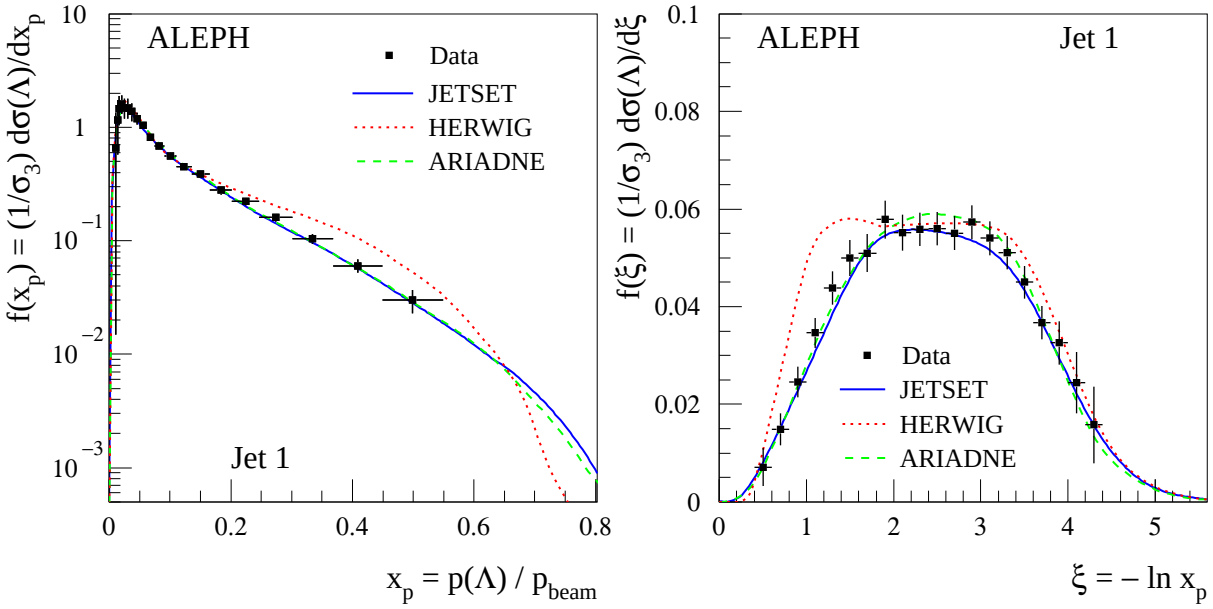

Figure 17: The inclusive cross sections of Λ and $\overline{\Lambda}$ in the first jet of the three-jet events in $x_p = p(\Lambda)/p_{\rm beam}$ and $\xi = -\ln x_p$. The error bars show the total errors (statistical and systematic errors added in quadrature).

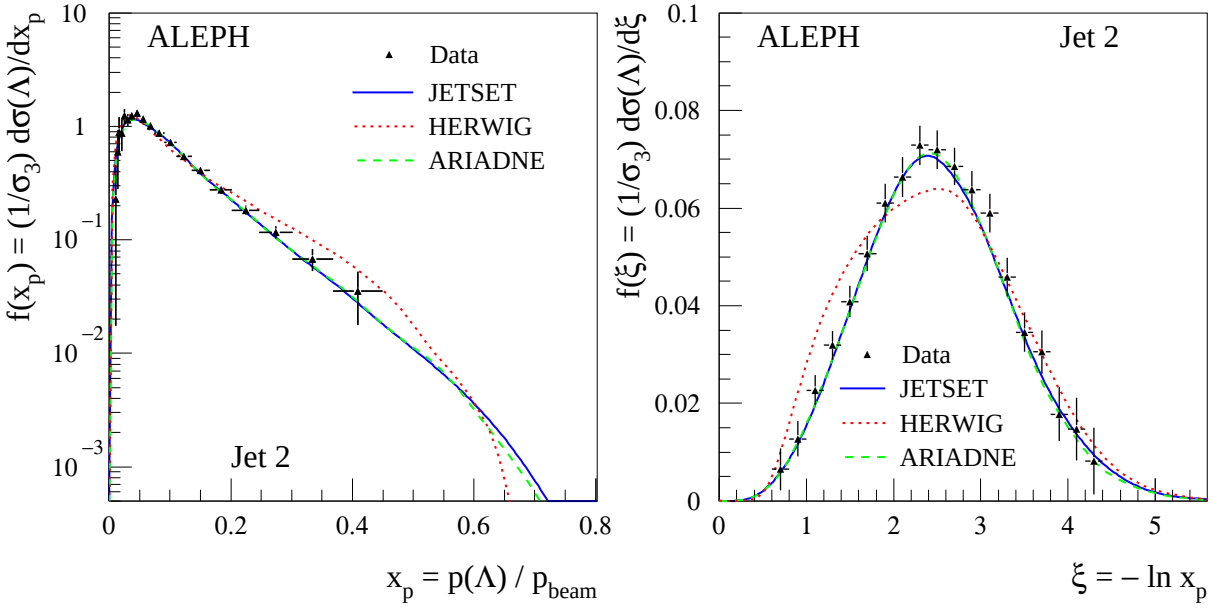

Figure 18: The inclusive cross sections of Λ and $\overline{\Lambda}$ in the second jet of the three-jet events in $x_p = p(\Lambda)/p_{\rm beam}$ and $\xi = -\ln x_p$. The error bars show the total errors (statistical and systematic errors added in quadrature).

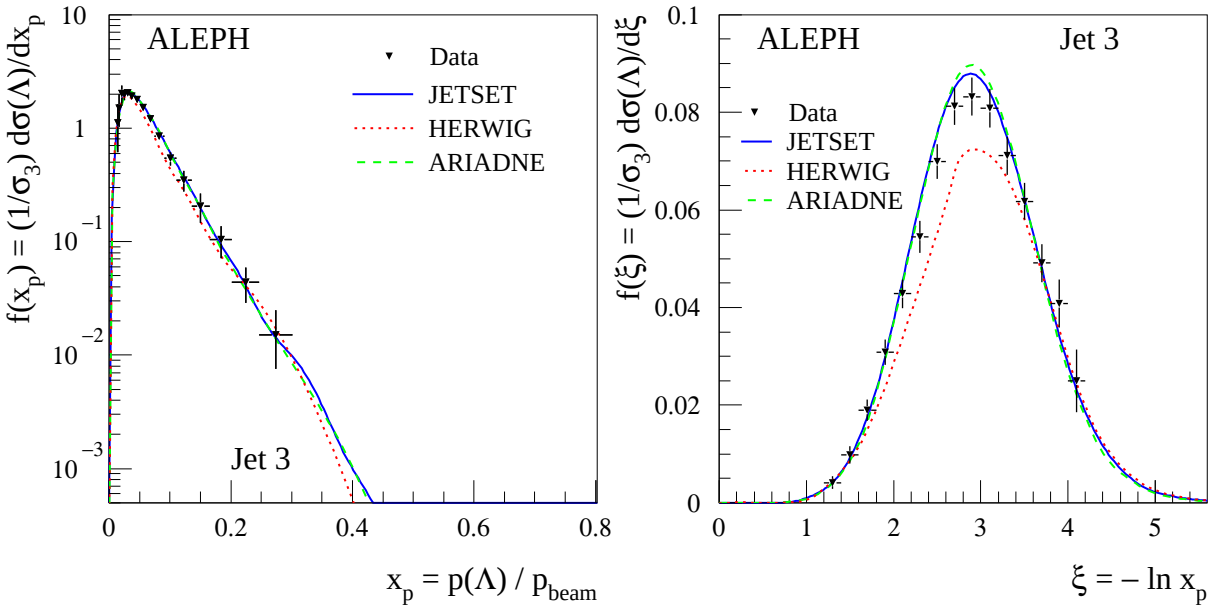

Figure 19: The inclusive cross sections of Λ and $\overline{\Lambda}$ in the third jet of the three-jet events in $x_p = p(\Lambda)/p_{\rm beam}$ and $\xi = -\ln x_p$. The error bars show the total errors (statistical and systematic errors added in quadrature).